Nanotechnology, Science and Applications

Dovepress

open access to scientific and medical research

Open Access Full Text Article

ORIGINAL RESEARCH

Green Nanotechnology of *Yucca filamentosa*-Phytochemicals-Functionalized Gold Nanoparticles—Antitumor Efficacy Against Prostate and Breast Cancers

Velaphi C Thipe[1,2], Ananya Jatar[1], Alice Raphael Karikachery[1,2], Kavita K Katti[1,2], Kattesh V Katti[1–4]

[1]Institute of Green Nanotechnology, University of Missouri, Columbia, MO, 65212, USA; [2]Department of Radiology, University of Missouri, Columbia, MO, 65212, USA; [3]Department of Physics, University of Missouri, Columbia, MO, 65211, USA; [4]Department of Medical Pharmacology and Physiology, University of Missouri, Columbia, MO, 65212, USA

Correspondence: Kattesh V Katti, Institute of Green Nanotechnology and Cancer Nanotechnology, Department of Radiology, Department of Physics, Department of Medical Pharmacology and Physiology, University of Missouri, Columbia, MO, USA, Tel +1 573 882-5656, Fax +1 573 884-5679, Email KattiK@health.missouri.edu

Purpose: We report an innovative green nanotechnology utilizing an electron-rich cocktail of phytochemicals from *Yucca filamentosa* L. to synthesize biocompatible gold nanoparticles without the use of any external chemical reducing agents and evaluate their anti-cancer activity.

Methods: *Yucca filamentosa* L. extract, containing a cocktail of phytochemicals, was prepared, and used to transform gold salt into *Y. filamentosa* phytochemicals encapsulated gold nanoparticles (YF-AuNPs). Additionally, gum arabic stabilized YF-AuNPs (GAYF-AuNPs) were also prepared to enhance the in vitro/in vivo stability. Anticancer activity was evaluated against prostate (PC-3) and breast (MDAMB-231) cancer cell lines. Targeting abilities of gold nanoparticles were tested using pro-tumor macrophage cell lines.

Results: Comprehensive characterization of new nanomedicine agents YF-AuNPs and GAYF-AuNPs revealed spherical, and monodisperse AuNPs with moderate zeta potentials (−19 and −20 mV, respectively), indicating in vitro/in vivo stability. The core size of YF-AuNPs (14 ± 5 nm) and GAYF-AuNPs (10 ± 5 nm) is suitable for optimal penetration into tumor cells through both enhanced permeability and retention (EPR) effect as well as through the receptor mediated endocytosis. Notably, YF-AuNPs exhibited potent anticancer activity against prostate (PC-3) and breast tumors (MDAMB-231) by inducing early and late apoptotic stages. Moreover, YF-AuNPs resulted in elevated levels of anti-tumor cytokines (TNF-α and IL-12) and reduced levels of pro-tumor cytokines (IL-6 and IL-10), provide compelling evidence on the immunomodulatory property of YF-AuNPs.

Conclusion: Overall, these *Y. filamentosa* phytochemicals functionalized nano-Ayurvedic medicine agents demonstrated selective toxicity to cancer cells while sparing normal cells. Most notably, to our knowledge, this is the first study that shows YF-AuNP's targeting efficacy toward pro-tumor macrophage cell lines, suggesting an immunomodulatory pathway for cancer treatment. This work introduces a novel avenue for herbal and nano-Ayurvedic approaches to human cancer treatment, mediated through selective efficacy and immunomodulatory potential.

Keywords: *Y. filamentosa*, phytoconstituents, gold nanoparticles, anticancer

Introduction

The World Health Organization has forecast that nearly 80% of the global population will use herbal and related holistic medicines in some form to alleviate pain and suffering from various diseases and disorders.[1] However, the limited bioavailability of therapeutically important herbs and their extracts has impeded the growth of herbal medicine as a reliable medical modality. We have a long-standing interest in improving bioavailability and realizing the tremendous potential of herbal medicine for treating debilitating human diseases effectively. Toward this quest, we have pioneered the development of green nanotechnology for its use as an innovative delivery vehicle to enhance the bioavailability of

Received: 30 August 2023
Accepted: 29 November 2023
Published: 11 December 2023

Graphical Abstract

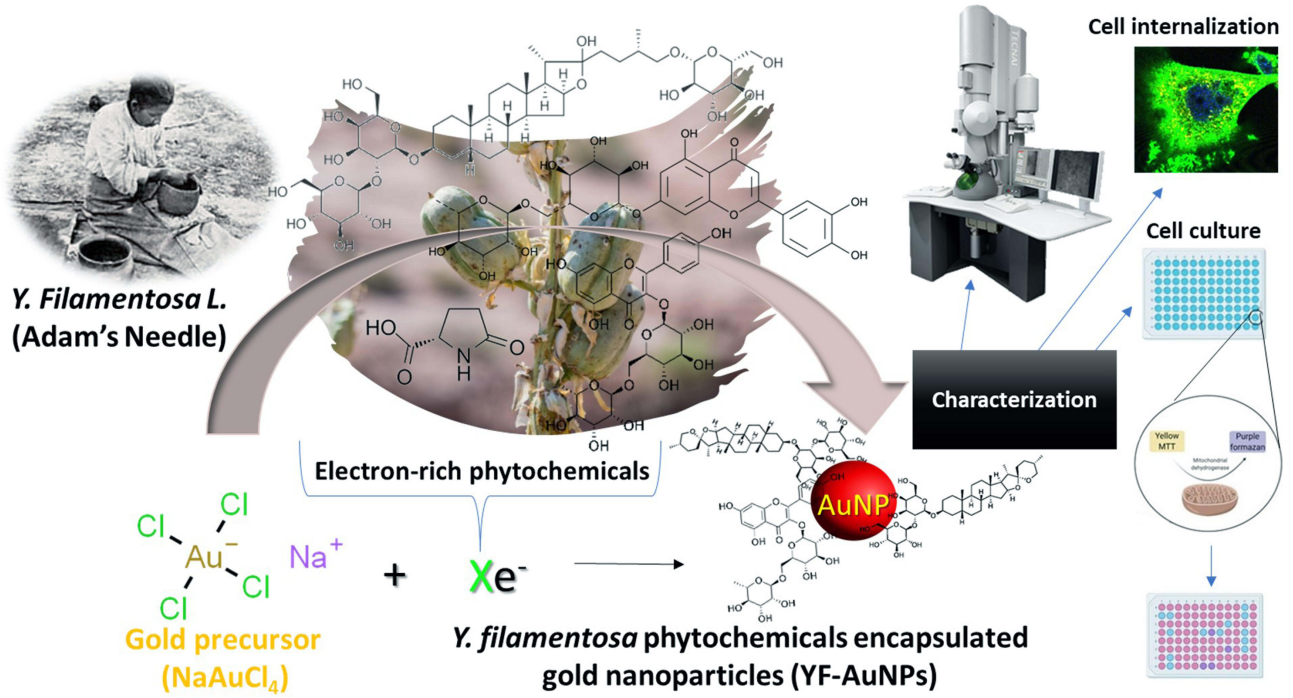

various bioactive and therapeutic phytochemicals from a plethora of plants.[2–21] Recent investigations have revealed that encapsulation of phytochemicals on gold nanoparticle surface not only enhances their bioavailability in vivo but the optimum size(s) of phytochemical(s) embedded gold nanoparticles allows target-specific delivery of phytochemicals—thus affording both selectivity and effective bioavailability.[15,16,22–25] In continuation of efforts to expand the rich therapeutic potential of phytochemicals from the plant kingdom, we have now focused on the utility of *Yucca* genus plants which consist of approximately 50 species of the Asparagaceae family, widespread in the southwestern United States, Mexico, and in the Caribbean. This genus is indigenous to the deserts of eastern North America and Florida.[26] It is important to recognize that *Y. schidigera* and *Y. Filamentosa* can grow in arid environments, thus making it a potential asset in the face of dangerous climate changes caused by global warming such as record increasing ambient temperatures, prolonged drought, and irregular patterns of rainfall. Historically, the *Yucca* genus has been used by indigenous Cherokee and the Catawba Indians in folk medicine to treat joint pain, asthma, bleeding, rheumatism, gonorrhea, sunburns, arthritis, prostate, and urethral inflammations.[27]

Adegbeye et al[28] reported on the importance of *Yucca* extract as feed additives because their phytochemicals can reduce methane by 8%–69%, total ammonia nitrogen in water by 50%–100%, nitrous oxide emissions by 75% while reducing nutrient digestibility and thereby reducing livestock environmental footprint. *Yucca* products have found utility as animal feed additives, food supplements, para-pharmaceutical complements, foaming agent in beverages, moisturizing agents, and as crop growth stimulants. The Food and Drug Administration of the United States (FDA) has approved the use of phytochemicals from *Yucca* in humans and are Generally Recognized As Safe (GRAS) certified.[29,30] The roots of *Y. filamentosa* are used in soaps due to spirostanol saponins, while various phytochemicals of *Y. filamentosa* have shown utility in treating osteoarthritis, high blood pressure, migraine headaches, inflammation of the intestine (colitis), arthritis, high blood cholesterol, stomach disorders, diabetes, liver and gallbladder disorders, as well as in cardiovascular health and also for healthy gut digestion.[30]

As part of our ongoing interest in developing "Zero-Carbon" footprint medical technologies and toward realizing the therapeutic potential of a myriad of native plants. We have recently shown that gold nanoparticles encapsulated with mangiferin—a phytochemical found in mango peel—provides immunomodulatory effects through elevated levels of pro-inflammatory cytokines such as Interleukin-12 (IL-12) and tumor necrosis factor alpha (TNF-α) generating M1-like macrophage cell lines that facilitate antitumor activity with subsequent reduction levels of anti-inflammatory cytokines, Interleukin-10 (IL-10) and Interleukin-6 (IL-6) to activate M2-like macrophage cell lines, also known as protumor macrophage cell lines as they promote tumor growth, as shown by extensive preclinical and clinical investigations.[15,17,22,24,31,32] This approach has created credible scientific relevance to over 5000-year-old Ayurvedic medicine while serving as genesis to a new medical modality referred to as nano-Ayurvedic medicine—for which the US Patents and Trade Marks office has granted the first ever patent.[33,34] Bolstered by the ability of gold nanoparticles in imparting optimum bioavailability and tumor cell specificity,[22,35–37] we hypothesized that encapsulation of phytochemicals from *Y. filamentosa* on gold nanoparticles will provide an effective delivery vehicle for use in cancer therapy.

As an experimental validation of our hypothesis, we herein, report: (i) green nanotechnology approaches for the synthesis and full characterization of gold nanoparticles using electron-rich phytochemicals from *Y. filamentosa* extracts to transform gold precursor into *Y. filamentosa* phytochemicals encapsulated gold nanoparticles (YF-AuNPs and GAYF-AuNPs); (ii) extensive biocompatibility investigations elucidating optimum in vitro/in vivo stability in biological media; (iii) tumor specificity of YF-AuNPs and GAYF-AuNPs through internalization of these nanoparticles into the cytoplasm; and (iv) excellent antitumor features of YF-AuNPs and GAYF-AuNPs against PC-3 and MDAMB-231 cancer cells, including evidence on the ability of these new nanomedicine agents to target and polarize M2-like macrophage cell line to M1-like macrophage cell line that can unleash anti-tumor immune responses.

Materials and Methods

Materials

In the present study, flower buds of *Y. filamentosa* (50 g) were collected from the University of Missouri, Columbia campus, USA. The plant was identified and authenticated by Dr K. H. Clary. A voucher specimen (BC:MO-2267845/A:3345883) was obtained from the Missouri Botanical Garden Herbarium. Metal precursor: 99% sodium tetrachloroaurate(III) dihydrate ($NaAuCl_4 \cdot 2H_2O$) was procured from Alfa Aesar (Heysham, UK). Biological media: DL-cysteine 97% (Cys), bovine serum albumin (BSA), gum arabic (GA), human serum albumin (HSA) lyophilized powder, sodium chloride (NaCl), phosphate buffered saline (PBS), and Hanks' balanced salt solution (HBSS) were all procured from Sigma-Aldrich (St Louis, MO, USA). Cellular stains: 4',6-diamidino-2-phenylindole (DAPI), L-histidine 98% (His), 3-(4,5-dimethylthiazol-2-yl)-2,5-diphenyltetrazolium bromide (MTT), lipopolysaccharide (LPS), wheat germ agglutinin (WGA) Oregon Green® 488 conjugate, WGA Alexa Fluor™ 680 conjugate, and trypan blue were procured from Sigma-Aldrich (St Louis, MO, USA). Positive control drugs: cisplatin sourced from US Pharmacopeia, Rockville, MD. Cellular culture: TrypLE Express procured from Thermofisher Scientific (Waltham, MA, USA), while fetal bovine serum (FBS), gentamicin, enzyme-linked immunosorbent assay (ELISA) kits: Tumour Necrosis Factor alpha (TNF-α), Interleukin-6 (IL-6), Interleukin-10 (IL-10), Interleukin-12 (IL-12). Dulbecco's Modified Eagle Medium (DMEM), Roswell Park Memorial Institute (RPMI) 1640, vascular cell basal medium (VCBM), and endothelial cell growth kit-VEGF were obtained from Life Invitrogen (New York, NY, USA). GFP-CERTIFIED Apoptosis/ Necrosis detection kit was obtained from Enzo Life Sciences, USA. Cell lines: Breast mammary gland adenocarcinoma (MDAMB-231), prostate adenocarcinoma (PC-3) cells, human aortic endothelial cells (HAEC), and murine macrophage (RAW 264.7) cell lines were obtained from the American Type Culture Collection (ATCC, Manassas, VA, USA).

Y. filamentosa Extract Preparation

About 0.3 g/mL of *Y. filamentosa* extract (BC:MO-2267845/A:3345883) was prepared by weighing 13 g large flower buds (cut into small pieces) of *Y. filamentosa* into a beaker. To it 50 mL of distilled water was added. The beaker contents

were heated to 100°C for 15 min and then allowed to cool to room temperature. It was then filtered using a stainless-steel Valerie double layered mesh sieve to obtain the *Y. filamentosa* extract solution.

Liquid Chromatography with Tandem Mass Spectrometry (LC-MS/MS)

Liquid chromatography with tandem mass spectrometry (LC-MS/MS) analysis was performed on a Bruker maXis impact quadrupole-time-of-flight mass spectrometer coupled to a Waters ACQUITY UPLC (ultrahigh performance liquid chromatography) system (UPLC-Q-TOF-MS/MS). Separation was achieved on a Waters C_{18} column (2 × 150 mm, BEH C_{18} column with 1.7 µm particles) using a linear gradient and mobile phase A (0.1% formic acid) and B (acetonitrile). Gradient condition was the following: B increased from 5% to 70% over 30 minutes, then to 95% over 3 minutes, held at 95% for 3 minutes, then returned to 5% for equilibrium. The flow rate was 0.6 mL/minute, and the column temperature was 60 °C.

Mass spectrometry was performed in the positive electrospray ionization mode with the nebulization gas pressure at 44 psi, dry gas of 12 L/min, dry temperature of 250°C and a capillary voltage of 4000 V. Auto MS/MS Mass spectral data were collected using the following parameters: MS full scan: 100 to 1500 m/z; number of precursors for MS/MS: 3; threshold: 10 counts; active exclusion: 3 spectra, released after 0.2 minutes; collision energy: dependent on mass, 10 eV at 50 Da, 20 eV at 200 Da, 30 eV at 500 Da, 40 eV at 1000 Da, and 50 eV at 1500 Da. The MS and MS/MS data were auto-calibrated using sodium formate that was introduced at the end of the gradient after data acquisition.

Y. filamentosa extract was centrifuged at 13,000 g for 15 min. After centrifugation, 2 µL of the supernatant was transferred to sample inserts and analyzed. Data were processed using MetaboScape (Bruker) software. Metabolites were putatively identified by matching their tandem spectral data against a custom tandem spectral library,[38] RIKEN spectral library, and NIST20 high resolution accurate mass library. Multivariate analysis was performed using MetaboAnalyst.

Gold Nanoparticle Synthesis Using *Y. filamentosa* Extract

To a 20 mL scintillation vial, 6 mL of the *Y. filamentosa* extract was added. The solution was stirred at 700 rpm and heated to 90°C. Then, 100 µL of 0.1 M $NaAuCl_4.2H_2O$ was added. The solution changed from a light yellow to a ruby red color indicating the formation of gold nanoparticles. The *Y. filamentosa* gold nanoparticles (YF-AuNPs) were washed twice by centrifugation using Fisherbrand™ accuSpin™ Micro 17/17R Microcentrifuge (Thermo Fisher Scientific, Waltham, MA, USA) operated at 13,300 rpm at 15°C for 15 min. YF-AuNPs were reconstituted in distilled water and characterized using Cary 60 UV–vis absorption spectroscopy (Agilent Technologies, Inc., Santa Clara, CA, USA), Zetasizer Nano ZS90 (Malvern Panalytical Inc., Westborough, MA, USA), Nicolet 4700 Fourier-transform infrared spectroscopy (FTIR) (Thermo Scientific, Inc., Waltham, MA, USA), Rigaku Ultima IV X-ray powder diffractometer (XRD) (Rigaku Americas Corporation, Woodlands, TX, USA), JEOL JEM-1400 120 kV transmission electron microscopy (JEOL Ltd., Peabody, MA, USA). Gum arabic stabilized *Y. filamentosa* gold nanoparticles (GAYF-AuNPs) were synthesized by dissolving 24 mg of gum arabic in a solution mixture containing 6 mL of *Y. filamentosa* extract and 6 mL distilled water. The solution was stirred at 700 rpm and heated to 90°C and 200 µL of 0.1 M $NaAuCl_4.2H_2O$ was added to produce GAYF-AuNPs and characterized like YF-AuNPs.

In vitro Stability Study of YF-AuNPs and GAYF-AuNPs

In the presence of diverse biological fluids (eg, 0.5% BSA, HSA, cysteine, 0.2 M histidine, 1% NaCl, RPMI and DMEM media, PBS at pH 5, 7 and 9); the in vitro stability of the YF-AuNPs and GAYF-AuNPs was examined. Briefly, 200 µL of YF-AuNPs or GAYF-AuNPs was mixed with 100 µL of each biological solution, followed by room-temperature incubation for a week. The stability was determined by UV–vis spectrophotometry by recording the surface plasmon resonance peak of YF-AuNPs and GAYF-AuNPs.

Cellular Uptake of YF-AuNPs

Cellular internalization endocytosis study of YF-AuNPs was performed. Briefly, coverslips that were ultraclean and sterile were placed in 6-well polystyrene-coated flat-bottomed plates, and 8×10^5 cells per well were seeded in media (DMEM for MDAMB-231 and RAW 264.7, RPMI for PC-3 cells, and VCBM for HAEC cells) and cultured for 24 hours

at 37°C in a 5% CO_2 incubator. After incubation, the media was aspirated and incubated at 37°C for 24 hours with media containing 50 µg/mL of YF-AuNPs. Following incubation, the cells were rinsed three times with 1X HBSS, and the cells were labeled with 2 µg/mL WGA to stain the cytoplasm and incubated for 10 minutes at room temperature in the dark. Cells were washed with 1X HBSS twice and permeabilized with 0.2% Triton X-100 at room temperature for 5 minutes. Cells were washed twice with 1X HBSS and stained with DAPI dye for staining the nucleus. Images were collected at 40 magnification, using Leica TCS SP8 STED confocal microscopy (Leica, Wetzlar, Germany). Dage Imaging Software was used to collect images. Additionally, cells (8×10^5 cells/mL) were grown in 6-well polystyrene-coated flat-bottomed plates, washed with 1X PBS, and incubated at 37°C for 24 hours with media containing 50 µg/mL of YF-AuNPs. After incubation, cells were washed with 1X PBS, cells were dislodged using Tryple E for 3 min and media added to stop trypsinization. The cells were collected into 1 mL Eppendorf tubes, centrifuged and washed with 1X PBS at 1000 rpm for 5 min. The cell pellets were mixed with 2% glutaraldehyde and 2% paraformaldehyde in 0.1 mM sodium cacodylate buffer. The cells were then treated with 1% osmium tetroxide in 2-mercaptoethanol, dehydrated in a range of acetone concentrations, and then embedded in Epon-Spurr epoxy resin. Using a diamond blade (Diatome, Hatfield, PA), 85-nm-thick sections were cut. For organelle visualization, the slices were stained with Sato's triple lead stain and 5% aqueous uranyl acetate. The samples were analyzed on a JEOL 1400 TEM microscope (JEOL, Peabody, Massachusetts) operating at 80 kV at the Electron Microscopy Core Facility of the University of Missouri-Columbia.

In vitro Cell Viability Efficacy of YF-AuNPs

Using the MTT cell proliferation assay, YF-AuNPs were evaluated for their in vitro anti-cancer cell viability efficacy against breast (MDAMB-231) and prostate (PC-3) cancer cell lines, per the manufacturer's instructions. Additionally, the cellular viability of YF-AuNPs was evaluated against human aortic endothelial cells (HAEC) and murine macrophage (RAW 264.7) cell lines. Briefly, 100 µL of 5×10^3 cells/mL of each cell line was seeded into 96-well polystyrene-coated flat-bottomed plates, and the plates were incubated at 37°C for 24 hours in a CO_2 incubator with 5% CO_2 atmosphere. The cells were treated with various concentrations of YF-AuNPs (6–200 µg/mL). Cancer drug cisplatin, served as positive control, while untreated cells were negative control. The plates were incubated for 24, 48, and 72 hours. After incubation, 10 µL of MTT dye (5 mg/mL in PBS stock solution) was added, and the plates were incubated for 3–4 hours. Then, the purple formazan crystals were solubilized with DMSO solution. The intensity of the generated purple color was measured using a SpectraMax M2 microplate reader (Molecular Devices LLC, San Diego, CA, USA) operating at 570 nm wavelength.

The percentage of cell viability was determined using the following equation (Equation 1):

$$\%\ \text{cell viability} = \frac{(T_{Ab} - B_{Ab})}{(C_{Ab} - B_{Ab})} \times 100 \quad (1)$$

where T_{Ab} = absorbance of treatment, B_{Ab} = absorbance of blank (media), and C_{Ab} = absorbance of control (untreated cells). Half-maximal inhibitory concentration (IC_{50}) values were calculated using the GraphPad Prism Version 8 software.

Mechanistic Assessment of Tumor Cell Death

The PC-3 and MDAMB-231 cancer cells (8×10^5 cells per well) were seeded in 6-well polystyrene-coated flat-bottomed plates containing ultraclean coverslips until ~80% confluent. The cells were treated with YF-AuNPs and incubated for 24 h and then analyzed using the GFP-CERTIFIED Apoptosis/Necrosis detection kit according to the manufacturer's instructions. Briefly, the cells were incubated with the dual detection reagent for 10 min after treatment with either YF-AuNPs or apoptosis inducer staurosporine (STS) as a positive control, and untreated served as negative control. The slides were then prepared and visualized, using Leica TCS SP8 STED confocal microscopy (Leica, Wetzlar, Germany) equipped with a dual filter set for Cyanine-3 (excitation/emission: 550/570 nm), 7-AAD (excitation/emission: 546/647 nm), and GFP/FITC (excitation/emission: 488/514 nm). Dage Imaging Software was used to collect images.

Co-Culture Investigation of YF-AuNPs-Treated Macrophages and Measurements of Cytokines

PC-3 and MDAMB-231 cell lines (1×10^5 cells/well) were plated overnight in respective 6-well polystyrene-coated flat-bottomed plate for adherence. Following that, RAW 264.7 macrophage cell lines were treated for 18–24 hr with YF-AuNPs (22 µM) and labeled with a 2 µM WGA Alexa Fluor™ 680 conjugate. To avoid the direct influence of YF-AuNPs on cancer cells, the macrophage cell lines were collected and washed twice with 1XHBSS to eliminate unbound YF-AuNPs. To differentiate the proliferation of PC-3 and MDAMB-231 cells, they were labeled with 2 µM WGA Alexa Fluor™ 488 conjugate. For 72 hr, YF-AuNPs macrophages were then co-cultured with PC-3 cells and MDAMB-231 cells separately at the ratio of 1:10 (1 part of PC-3/MDAMB-231 cells to 10 parts of macrophages). The co-culture images were acquired using Leica SP8 spectral confocal microscopy. RAW 264.7 macrophage cell line supernatant and the co-culture (PC-3: RAW 264.7 and MDAMB: RAW 264.7) supernatant were collected for cytokine analysis. Briefly, the cells were cultured in 6-well polystyrene-coated flat-bottomed plates overnight and treated with YF-AuNPs for 4 h. Lipopolysaccharide (LPS) was used as positive and untreated as negative control. The cells supernatant was collected and analyzed for TNF-α, IL-6, IL-10 and IL-12 using ELISA kits.

Statistical Analysis

GraphPad Prism Version 8 software (GraphPad Software, San Diego, CA, USA) was used to conduct statistical analysis. Using the two-way ANOVA test, statistical evaluation was conducted to determine the efficacy of the treatment. To compare the average of the treatment group to the average of the control group, the IC_{50} was calculated. With $p < 0.05$ statistical tests were deemed significant. All results are shown as the mean standard error of the mean.

Results

Chemical Composition of *Y. filamentosa* by LC-MS/MS

LC-MS/MS data revealed that the major phytochemical chemical constituent is Timosaponin BII followed by arginine, L-pyroglutamic acid, glycosylated compounds, 3-alkylindoles, pyridine derivatives, and flavonoid-7-O-glycosides as shown in Figure 1. Timosaponin BII has been reported to have pharmacological activity for a variety of treatments including attenuating senile dementia, blood coagulation, tumor progression, osteoporosis, and inflammation.[39–41] The LC-MS/MS phytochemical composition pie chart of *Y. filamentosa* extract is shown in Figure 2. Flavonoid-3-O-glycosides including kaempferol 3-O-rutinoside (m/z 595.17, retention time 6 min) are also seen in minor quantities.

UV-Vis Spectroscopy and Physicochemical Properties of YF-AuNPs and GAYF-AuNPs

The ruby-red colors of YF-AuNPs and GAYF-AuNPs indicated the successful production of gold nanoparticles which was further corroborated by surface plasmon resonance (SPR) characteristic peaks at 536 nm and 540 nm, respectively (Figure 3). The reduction of cationic gold(III) (Au^{3+}) ions to gold zero-valent entity (Au^0) can be attributed to the high redox potential of the phytochemicals in the *Y. filamentosa* extract (Figure 4). The proposed mechanism involves oxidation of phenolic phytochemicals to the corresponding quinone derivatives enabling reduction of Au^{3+} ions to form YF-AuNPs (Figure 4) with robust surface coating and stabilization of other biomolecules such as arginine.[42–44] The functionalized YF-AuNPs and GAYF-AuNPs were further characterized by FTIR, the wavenumbers at 1639, 1631, 1641, 1672 cm^{-1} are assigned to carbonyl stretching (C=O) are attributed to the YF extracts and gum arabic suggesting conjugation for stabilizing YF-AuNPs and GAYF-AuNPs, respectively. The range at 3283 to 3573 cm^{-1} is associated with hydroxyl groups (O-H) stretching indicated by the interaction of gum arabic and YF extract phytochemicals with the gold nanoparticle surface, acting as stabilizing ligands for the nanoparticles (Figure 5a). The XRD analysis of GAYF-AuNPs and YF-AuNPs revealed four prominent peaks at 2θ values of 38.2°, 44.3°, 64.6°; 64.7°, and 77.5°; 77.7° (Figure 5b). These peaks align with the standard Bragg reflections (111), (200), (220), and (311) characteristic of the face-centered cubic (fcc) lattice structure for gold.

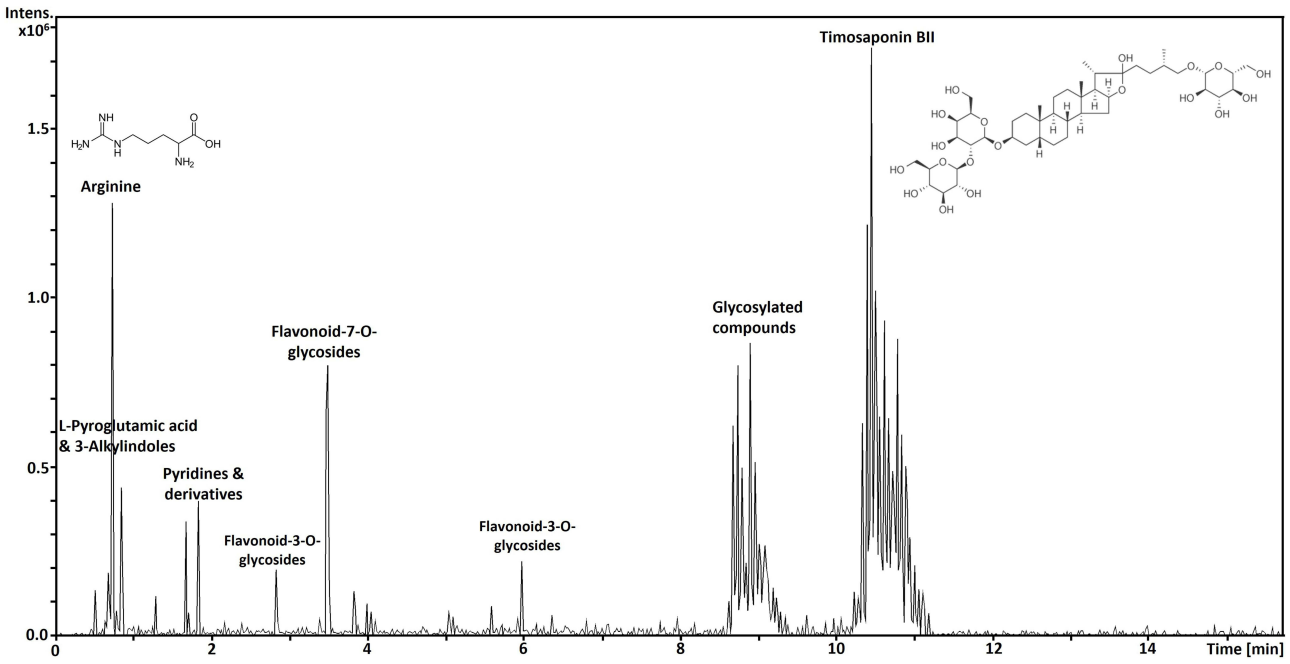

Figure 1 LC-MS/MS spectra of *Y. filamentosa* water extract.

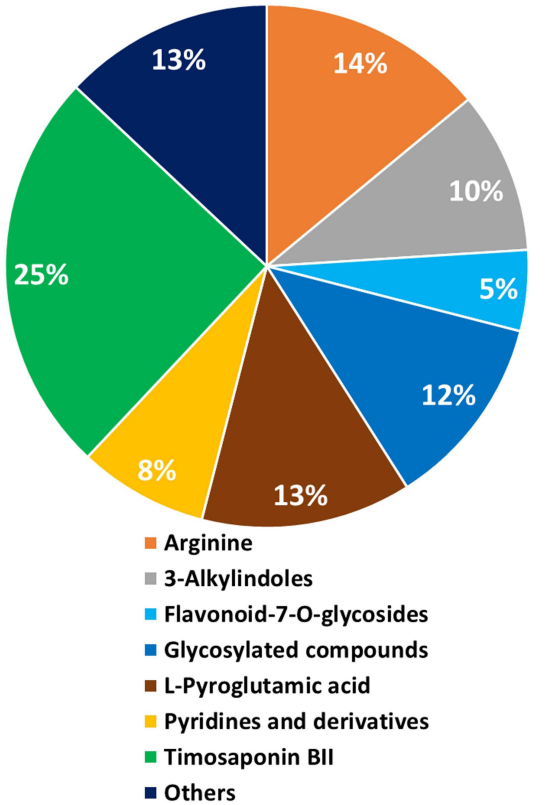

Figure 2 LC-MS/MS phytochemical composition pie chart of *Y. filamentosa* extract.

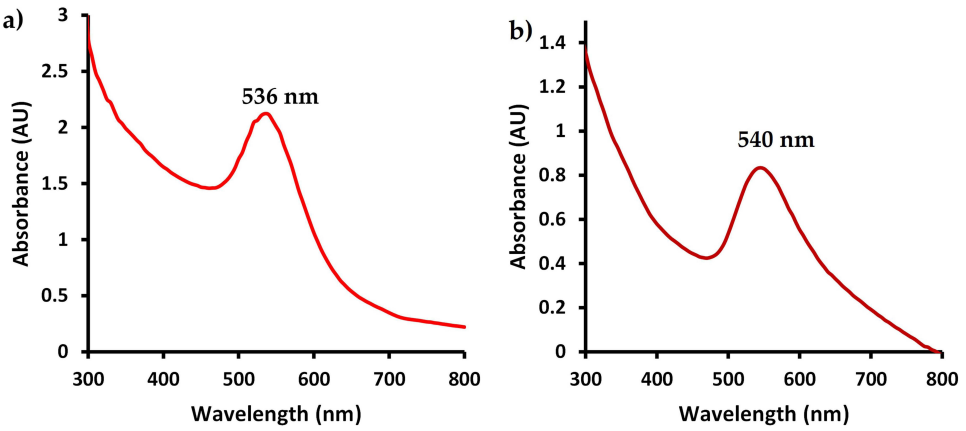

Figure 3 Ultraviolet-visible spectra of (**a**) YF-AuNPs and (**b**) GAYF-AuNPs.

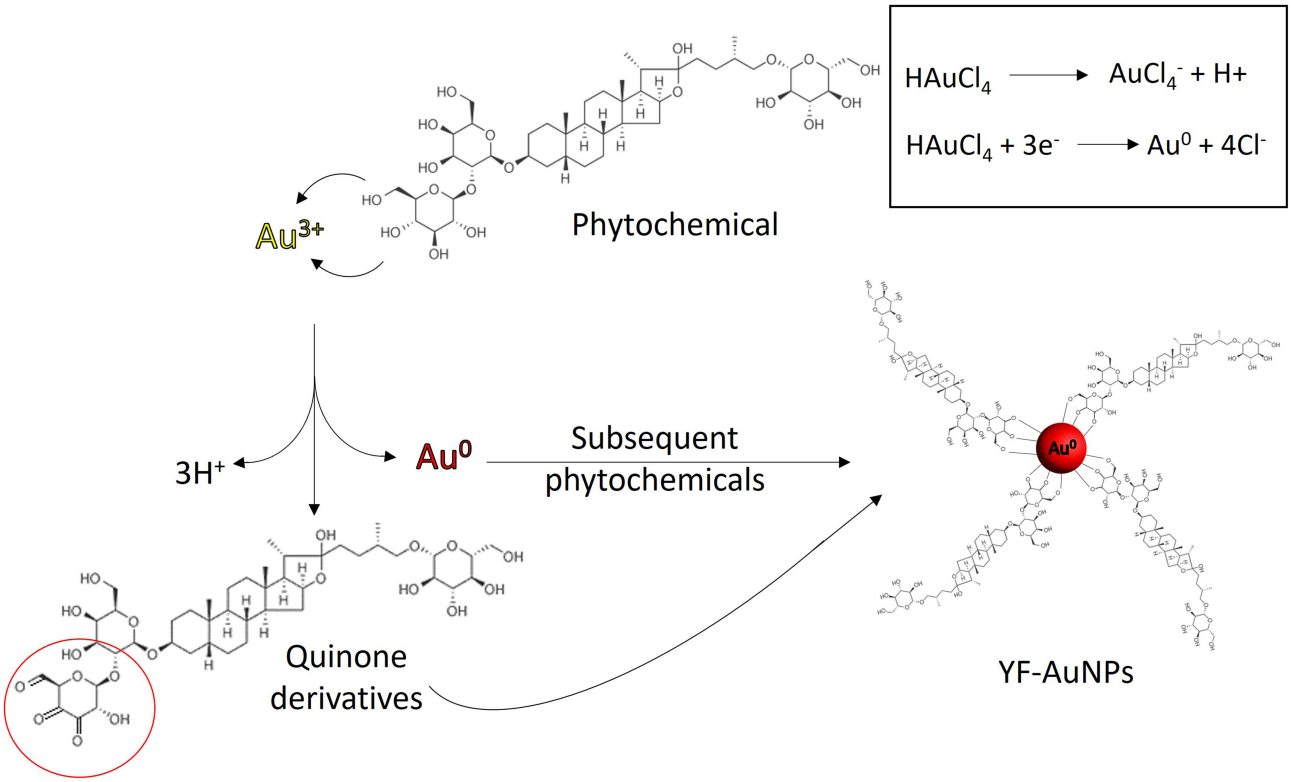

Figure 4 Proposed mechanism of *Y. Filamentosa* extract phytochemical oxidation to produce *Y. filamentosa* gold nanoparticles (YF-AuNPs) and the Au^{3+} reduction to Au^{0} nanoparticle.

In vitro Stability of YF-AuNPs and GAYF-AuNPs

In vitro stability measurements indicated no/minimal SPR peak shifts when incubated with various biological media (0.5% BSA, HSA, Cys, 0.2 M His, 1% NaCl, RPMI and DMEM media, PBS at pH 5, 7 and 9) for a period of 7 days (Figures 3 and 6). The physicochemical properties of YF-AuNPs and GAYF-AuNPs were evaluated using the Zetasizer which revealed that the hydrodynamic sizes were 335 ± 10 nm and 188 ± 5 nm with a polydispersity index (PDI) of 0.3 and 0.2, respectively. The zeta potentials of YF-AuNPs and GAYF-AuNPs were −19 mV and −20 mV, respectively, as shown in Table 1. The concentration of gold in YF-AuNPs and GAYF-AuNPs was 226 and 223 µg/mL, respectively (Table 1). This was calculated based on the amount of $NaAuCl_4.2H_2O$ utilized for the nanoparticle synthesis.

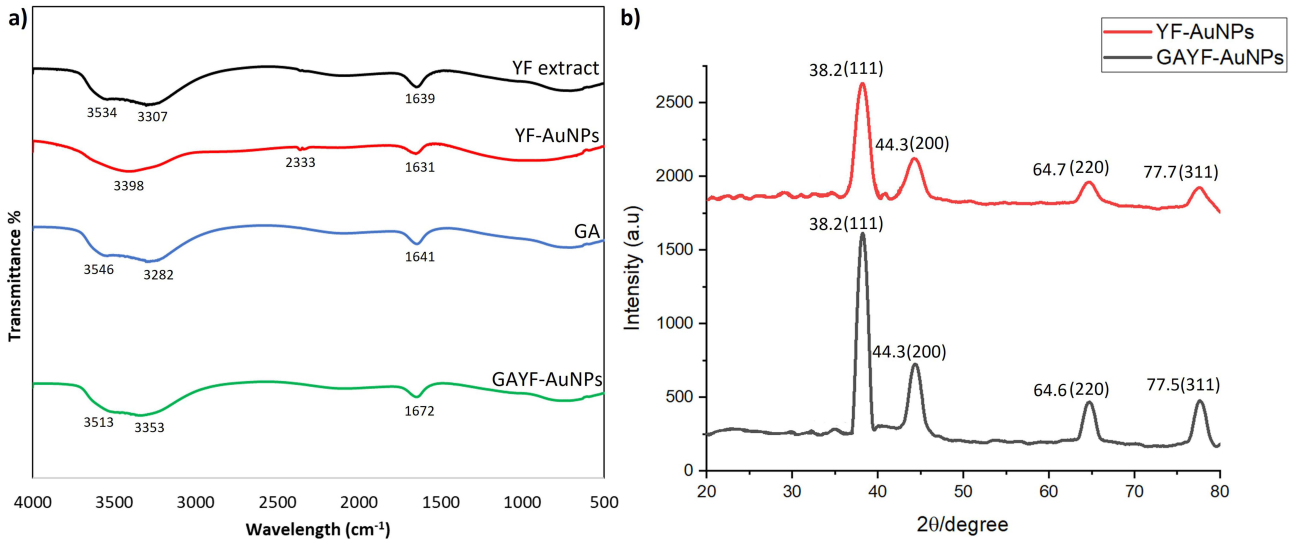

Figure 5 FTIR and XRD analysis of gold nanoparticles, (**a**) FTIR spectra indicated *Y. filamentosa* extract phytochemicals with the gold nanoparticle surface, acting as both a reducing and stabilizing ligand for the nanoparticles and (**b**) XRD spectra revealed crystalline nanoparticles represented by four peaks corresponding to standard Bragg reflections (111), (200), (220), and (311) of face-centered cubic lattice. The intense peak at 38.1 represents preferential growth in the (111) direction.

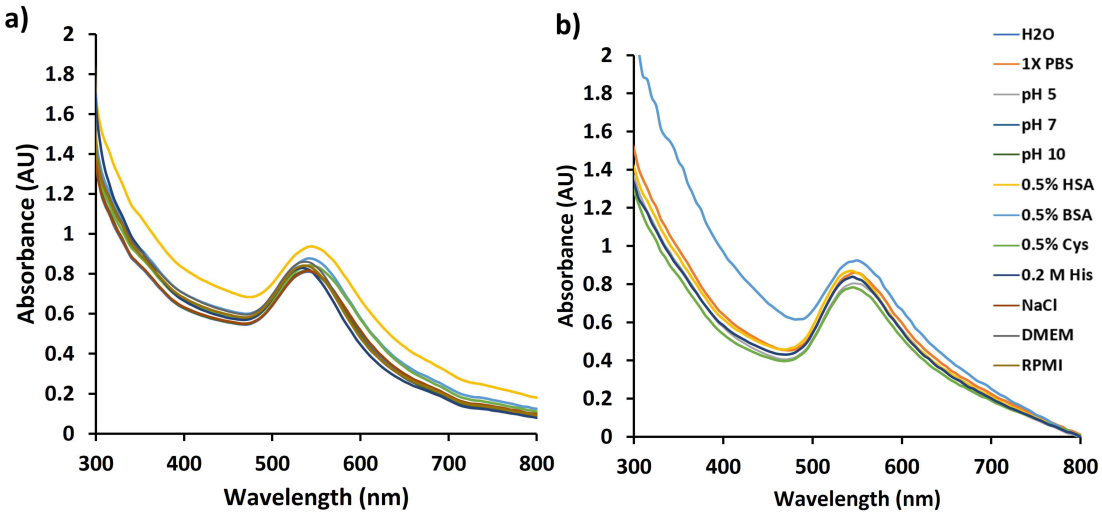

Figure 6 Ultraviolet-visible spectra for the in vitro stability of (**a**) YF-AuNPs and (**b**) GAYF-AuNPs.

Transmission Electron Microscopy (TEM) of YF-AuNPs and GAYF-AuNPs

The TEM images reveal that the average core size of YF-AuNPs and GAYF-AuNPs were 14 ± 5 and 10 ± 5 nm, respectively (Figure 7). The average core size was calculated from the size distribution analysis using Image J software. Additionally, TEM images further revealed that both YF-AuNPs and GAFY-AuNPs exhibited monodispersity with a spherical morphology. There was no significant size difference and both YF-AuNPs and GAFY-AuNPs exhibited similar in vitro stabilities. Therefore, we chose YF-AuNPs for detailed cellular investigations.

Cellular Internalization of YF-AuNPs

Figures 8 and 9 show cellular uptake of YF-AuNPs on the tested cell lines (PC-3, MDAMB-231, RAW 264.7, and HAEC cells). As depicted in Figures 8a and 9a, the YF-AuNPs showed excellent propensity to internalize into prostate tumor (PC-3) cell line and macrophage (RAW 264.7) cell line through endocytosis when compared to breast tumor (MDAMB-231) cells (Figure 8b) revealing that YF-AuNPs in addition of being tumor-specific also target macrophage cell lines

Table 1 Physicochemical Properties of YF-AuNPs and GAYF-AuNPs

Parameters	*Y. filamentosa* Gold Nanoparticles	
	YF-AuNPs	**GAYF-AuNPs**
Hydrodynamic size (nm)	335±10	188±5
Polydispersity index	0.3	0.2
Core size (nm)	14±5	10±5
Count rate (kcps)	250	243
Phytochemical coating (nm)	321	178
Zeta potential (mV)	−19	−20
Au concentration (µg/mL)	226	223

Abbreviations: YF-AuNPs, *Yucca filamentosa* L. gold nanoparticles; GAYF-AuNPs, Gum arabic-stabilized YF-AuNPs.

(Figure 9a). The multitude of *Y. filamentosa* phytoconstituents attached to the enormous surface area of gold allow for the delivery of a massive cargo of therapeutic phytochemicals, thus leading to the uptake of therapeutic nanoparticles by tumor cells. To demonstrate the tumor specificity of YF-AuNPs, we examined the cellular uptake of YF-AuNPs with

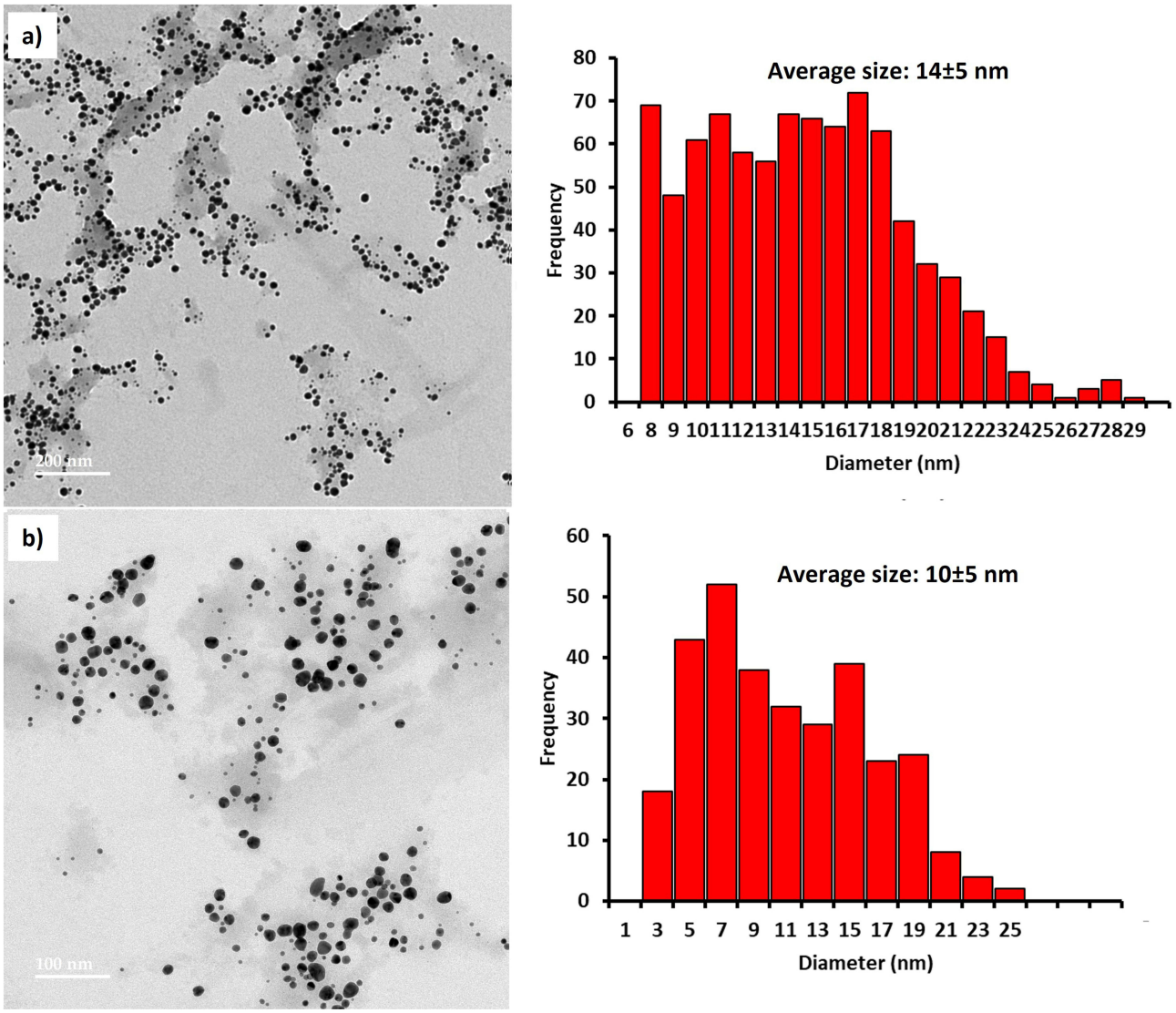

Figure 7 TEM image of (**a**) YF-AuNPs and (**b**) GAYF-AuNPs and size distribution graph.

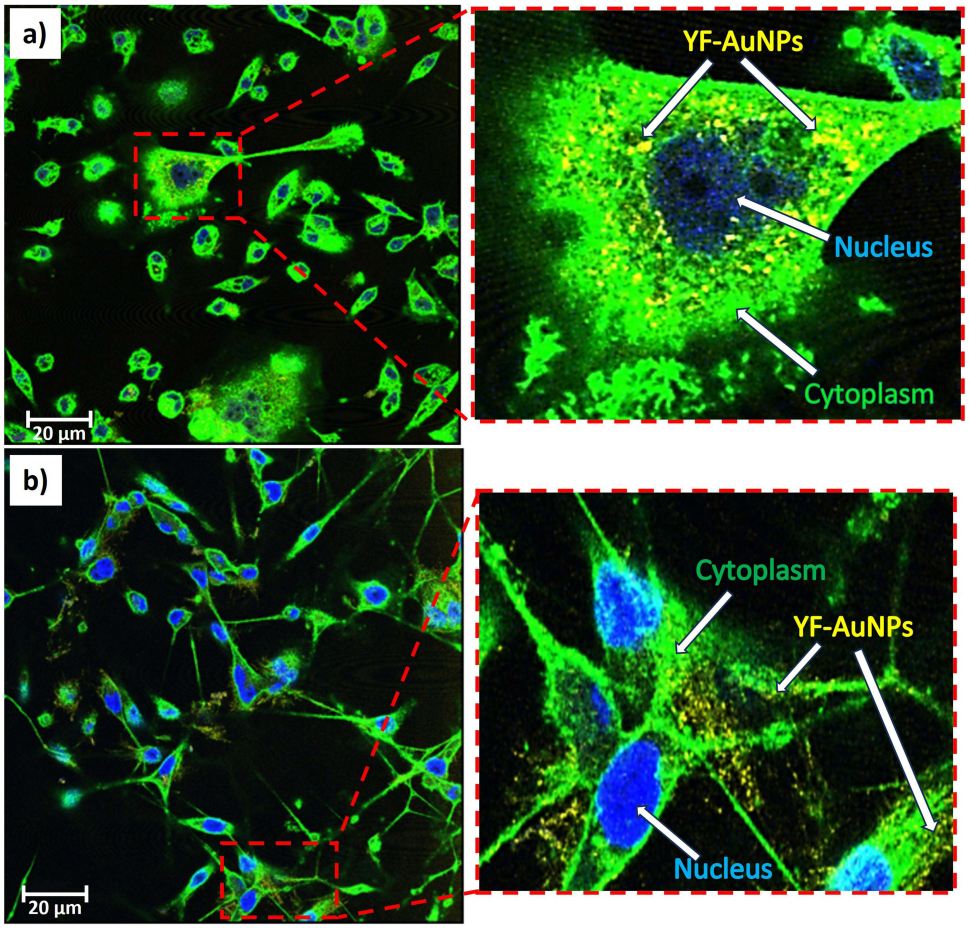

Figure 8 Confocal microscopy images of YF-AuNPs (50 µg/mL): cellular internalization in (**a**) PC-3 and (**b**) MDAMB-231 cells after 24 hr incubation. The cytoplasm (green – WGA labeling), nucleus (blue – DAPI stain) and YF-AuNPs (yellow) seen.

normal cells (HAEC) because they are non-cancerous cells, more mature, physiologically relevant, and more sensitive to drugs than human umbilical vein endothelial cells (HUVECs), thus making them valuable for assessing the potential toxicity of drugs. The results, as shown in Figure 9b, indicated that HAEC cells exhibited minimal to no uptake of YF-AuNPs. Additional investigations as shown in Figures 10 and 11 using electron microscopy, where Figures 10a and c and 11a and c show untreated PC-3, MDAMB-231, RAW 264.7, and HAEC cell lines, respectively. Tumor specificity of YF-AuNPs exhibited a significant propensity to internalize into PC-3 cells (Figure 10b), MDAMB-231 cells (Figure 10d), and RAW 264.7 cells (Figure 11b) clearly depicted by the vacuoles housing YF-AuNPs through endocytosis, while HAEC cells (Figure 11d) showed no YF-AuNPs cellular uptake. Furthermore, the size distribution of the internalized YF-AuNPs showed an average size of 14.8 ± 4.3, 15.7 ± 4.3 nm, and 17.5 ± 5.4 nm for PC-3, MDAMB-231, and RAW 264.7, respectively; illustrating the stability of YF-AuNPs to maintain their integrity (size and shape) inside the cells. These findings are significant in the context of YF-AuNPs' potential use as a tumor-specific therapeutic agent with minimal or no toxicity to normal cells.

Antitumor-Cellular Efficacy of YF-AuNPs

In keeping with our overall approach to avoid animal testing, in vitro antitumor efficacy of YF-AuNPs has been evaluated using breast (MDAMB-231) and prostate (PC-3) cancer cell lines for their potential to inhibit tumor cell growth. Cisplatin, a metal-based, FDA-approved, chemotherapeutic agent was used as a positive control. Antitumor assay data, as shown below, demonstrated conclusively that the antitumor effectiveness was concentration dependent. YF-AuNPs exhibited potent antitumor activity, which was comparable in potency to that of cisplatin, while

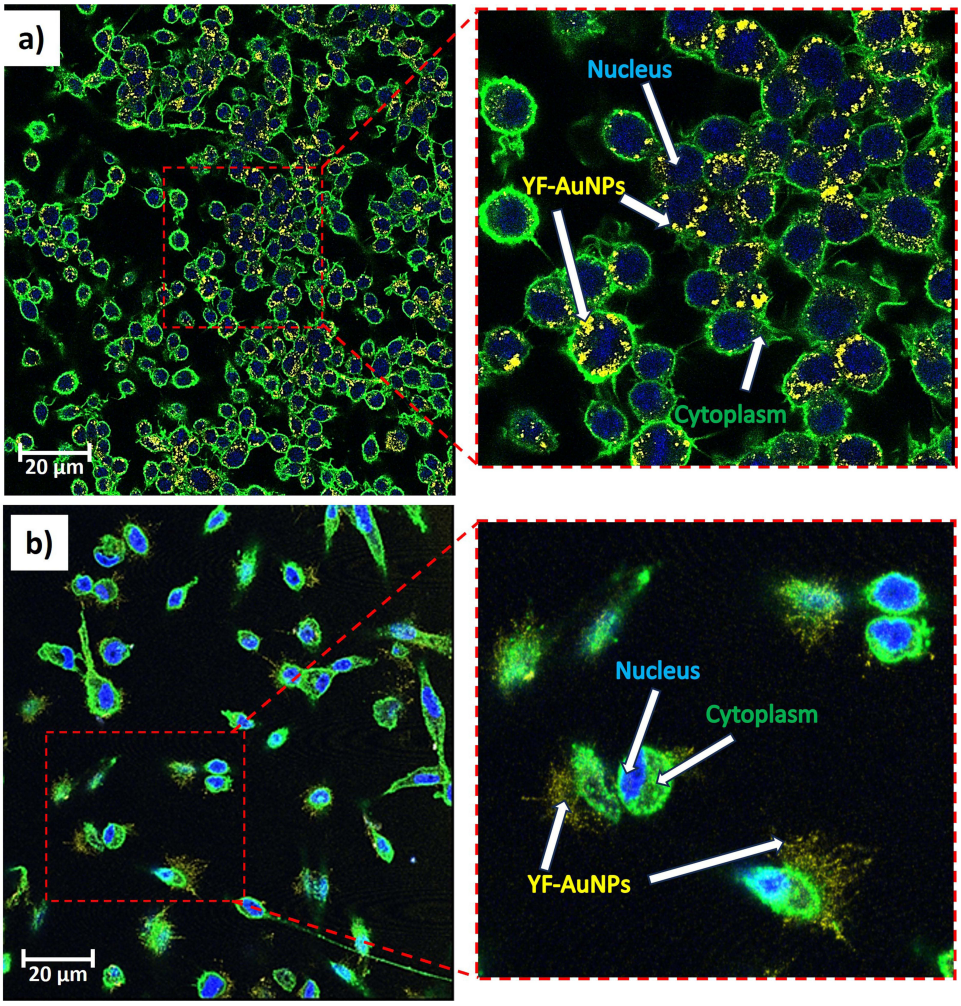

Figure 9 Confocal microscopy images of YF-AuNPs (50 µg/mL): cellular internalization in (**a**) RAW 264.7 and (**b**) HAEC cells after 24 hr incubation. The cytoplasm (green – WGA labeling), nucleus (blue – DAPI stain) and YF-AuNPs (yellow) seen.

demonstrating better toxicity against normal (HAEC) cells than cisplatin (Figures 12–14 and Table 2). The antitumor mechanism induced by YF-AuNPs on PC-3 and MDAMB-321 cell line was attributed to apoptosis as depicted in Figure 15. Cells treated with YF-AuNPs exhibited a significantly higher degree of apoptosis compared to untreated control (CTL) cells. These results demonstrate that YF-AuNPs exert early and late apoptotic stages, represented by yellow and red fluorescence, respectively. Notably, the pattern of apoptotic cell death induced by YF-AuNPs at 80 µM closely resembles that observed following treatment of cancer cells with the standard drug Staurosporine (STS). This confirms that YF-AuNPs trigger apoptosis in cancer cells, commencing with the early apoptotic phase and ultimately culminating in effective programmed cancer cell death.

Macrophage Cell Line Targeting and Immunomodulatory Characteristics of YF-AuNPs

It is well known that infiltration of macrophage cell lines in various tumors is associated with poor prognosis and has been attributed to be the root cause of resistance to chemotherapy and allied cancer therapies. Macrophage cell lines, within the tumor microenvironment, initiate rapid angiogenesis and catalyze tumor cells migration resulting in invasion and intravasation. These events, in tandem, cause immunosuppression at all stages of tumor progression—thus making targeting pro-tumor macrophage cell lines as an indispensable therapeutic approach in cancer therapy.[45–49] Macrophage cell lines, which account for close to 50% of stromal cells in the tumor microenvironment, often exhibit immunosuppressive M2-pro tumor phenotype in most cancers. There is a credible correlation of M2 phenotypes with tumor growth,

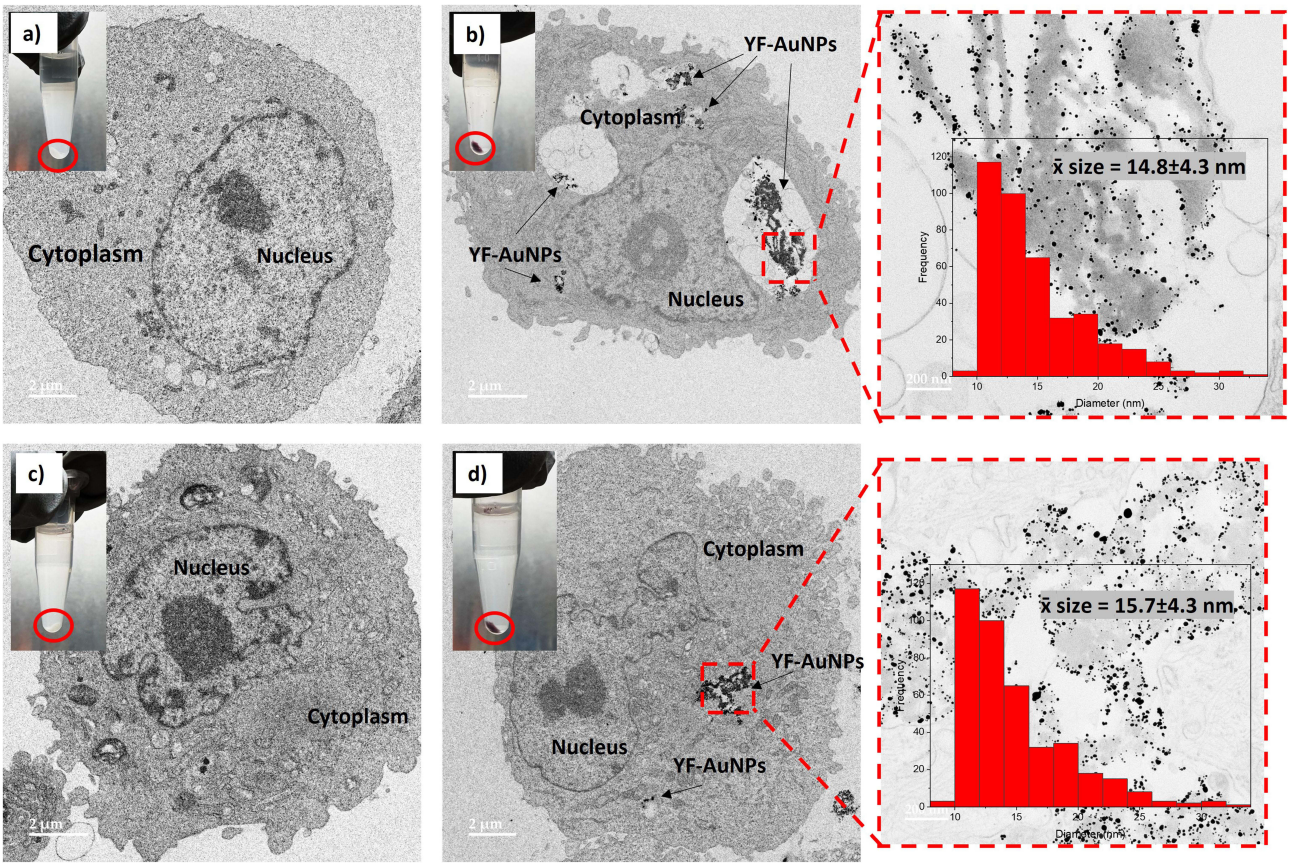

Figure 10 TEM images for cellular internalization (**a**) PC-3 (untreated control), (**b**) PC-3 treated with YF-AuNPs (50 µg/mL) 24 hr post-incubation, (**c**) MDAMB-231 (untreated control), and (**d**) MDAMB-231 treated YF-AuNPs (50 µg/mL) 24 hr post-incubation. The red circle indicates the color of the cell pellets and the size distribution of YF-AuNPs at 14.8±4.3 and 15.7±4.3 nm for PC-3 and MDAMB-231, respectively.

migration, angiogenesis, and immunosuppression. Various cancer cells, including prostate and breast, induce pro-tumor M2 polarization of RAW 264.7 macrophage cell lines. Therefore, RAW 264.7 macrophage cell lines present a reliable model for investigating tumor-associated macrophages (TAMs) aimed at understanding the targeting ability of various drugs, phytochemicals, and phytochemical-embedded nanoparticles for delineating important information on cancer-macrophage plasticity characteristics.[50–53] We have, therefore, chosen RAW 264.7 macrophage cell lines to investigate the ability of YF-AuNPs to target pro-tumor M2 macrophage cell lines. The results presented in Figures 9aand 11b, unequivocally, confirm that YF-AuNPs target pro-tumor macrophage cell lines effectively. To elucidate the impact of YF-AuNPs on RAW 264.7 macrophage cell lines, we carried out co-culture experiments with YF-AuNPs pre-treated RAW 264.7 macrophage cell lines incubation with either PC-3 or MDAMB-231 cell line to evaluate the cellular density as shown in Figure 16a–c, PC-3 and MDAMB-231 cells treated with naive macrophage cell line had a high cell density while cells treated with YF-AuNPs pretreated macrophage cell line had a low cell density (Figure 16b and d). Additionally, the levels of macrophage-polarizing cytokines (TNF-α, IL-6, IL-10, and IL-12) were measured. The results demonstrated that RAW 264.7 macrophages treated with YF-AuNPs resulted in elevated levels of anti-tumor cytokines (TNF-α and IL-12) and reduced levels of pro-tumor cytokines (IL-6 and IL-10) as shown in Figure 16e and f when compared to LPS that served as a positive control. These results corroborate the targeting and immunomodulatory characteristics of YF-AuNPs on RAW 264.7 macrophage cell lines and provide compelling evidence on the immuno-modulatory role of YF-AuNPs in treating various types of cancers.

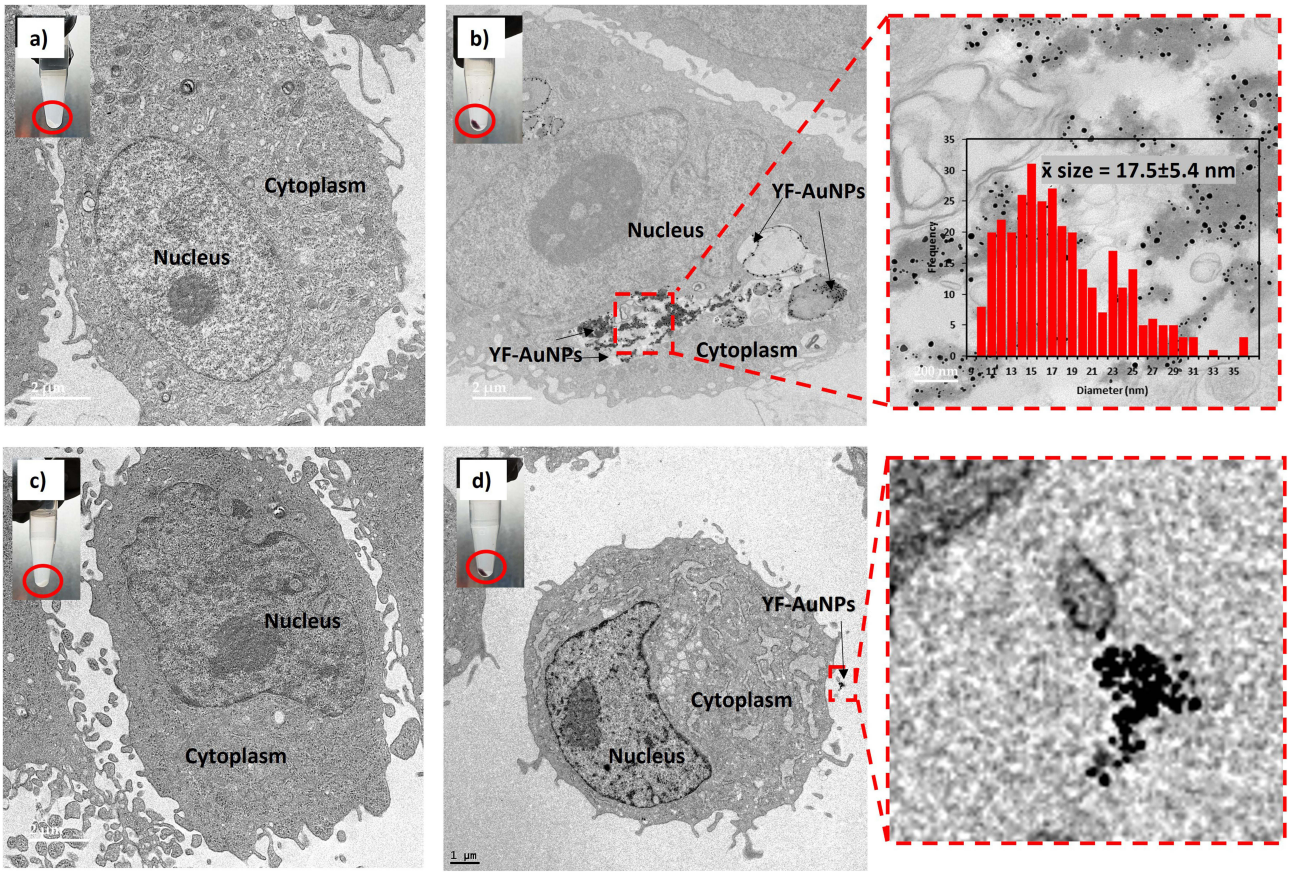

Figure 11 TEM images for cellular internalization (**a**) RAW 264.7 (untreated control), (**b**) RAW 264.7 treated with YF-AuNPs (50 µg/mL) 24 hr post-incubation, (**c**) HAEC (untreated control), and (**d**) HAEC treated YF-AuNPs (50 µg/mL) 24 hr post-incubation. The red circle indicates the color of the cell pellets and the size distribution of YF-AuNPs at 17.5±5.4 and YF-AuNPs located outside the HAEC cells, revealing no cellular internalization, respectively.

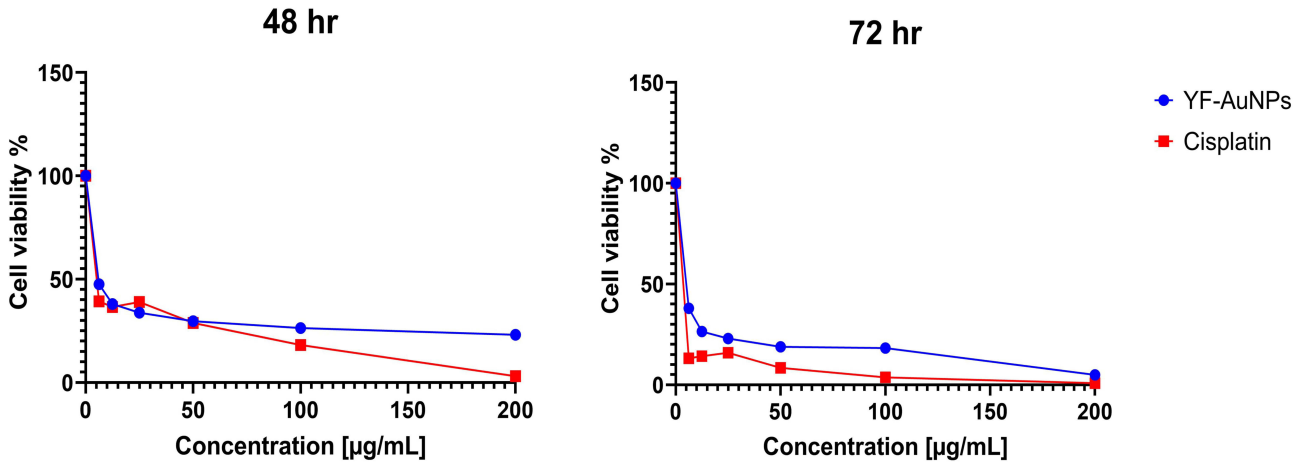

Figure 12 Anti-cancer efficacy of YF-AuNPs against PC-3 cells.

Discussion

The main objective of our investigation was to experimentally validate the hypothesis that electron-rich cocktail of phytochemicals found in *Y. filamentosa* can be used (i) in the transformation of gold precursors into their corresponding phytochemicals encapsulated biocompatible gold nanoparticles, through a green nanotechnology approach and without the use of any external toxic chemical reducing agents; (ii) harness the large surface area of gold nanoparticles for

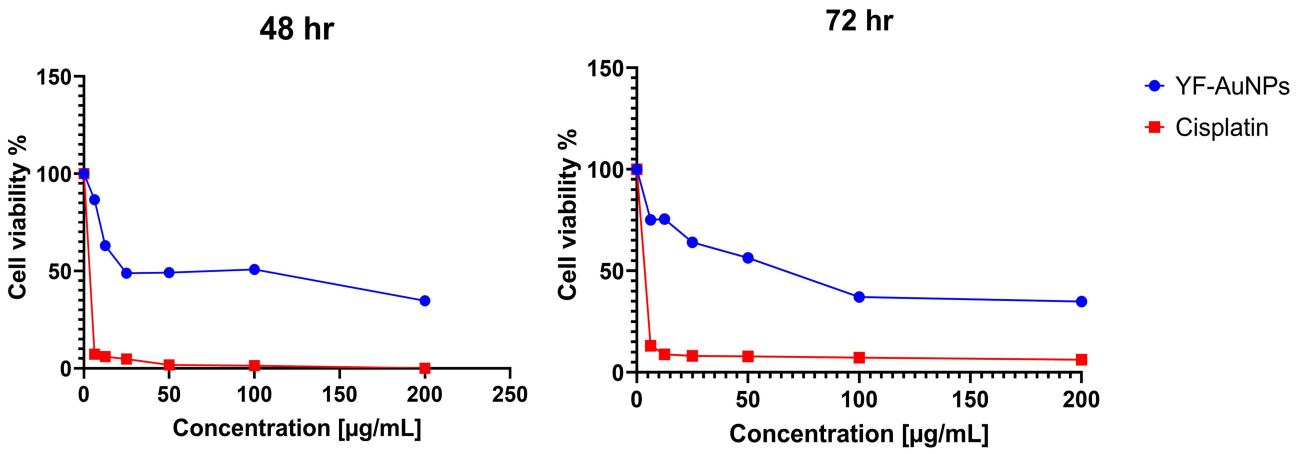

Figure 13 Anti-cancer efficacy of YF-AuNPs against MDAMB-231 cells.

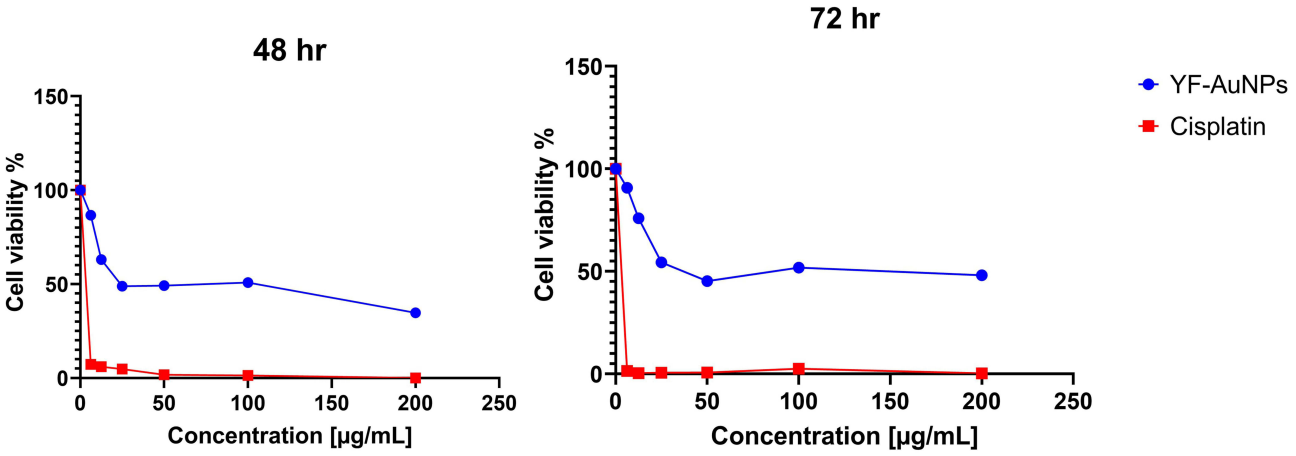

Figure 14 Anti-cancer efficacy of YF-AuNPs against HAEC cells.

incorporating high amounts of a plethora of therapeutic phytochemicals to achieve significant enhancement of delivering therapeutic cargo at tumor sites selectively and (iii) to examine the immunomodulatory properties of phytochemical-embedded gold nanoparticles in the immunotherapy of cancer. Highly antioxidant *Yucca* phytochemicals possess free-radical scavenging properties, which could inhibit reactive oxygen species and stop inflammatory responses. These phytochemicals have been studied for their ability to limit inducible nitric oxide synthase (iNOS) enzyme expression. In

Table 2 IC_{50} Values of YF-AuNPs and Cisplatin Against PC-3, MDAMB-231, and HAEC Cells

Cell Line	YF-AuNPs		Cisplatin	
	IC_{50} (µg/mL)		IC_{50} (µg/mL)	
	48 hr	72 hr	48 hr	72 hr
PC-3	19.7	11.6	8.6	5.5
MDAMB-231	23.5	78.4	53.2	5.1
HAEC	14.6	25.1	3.9	3.8

Abbreviation: IC_{50}, the concentration of a drug or inhibitor needed to inhibit a biological process or response by 50%.

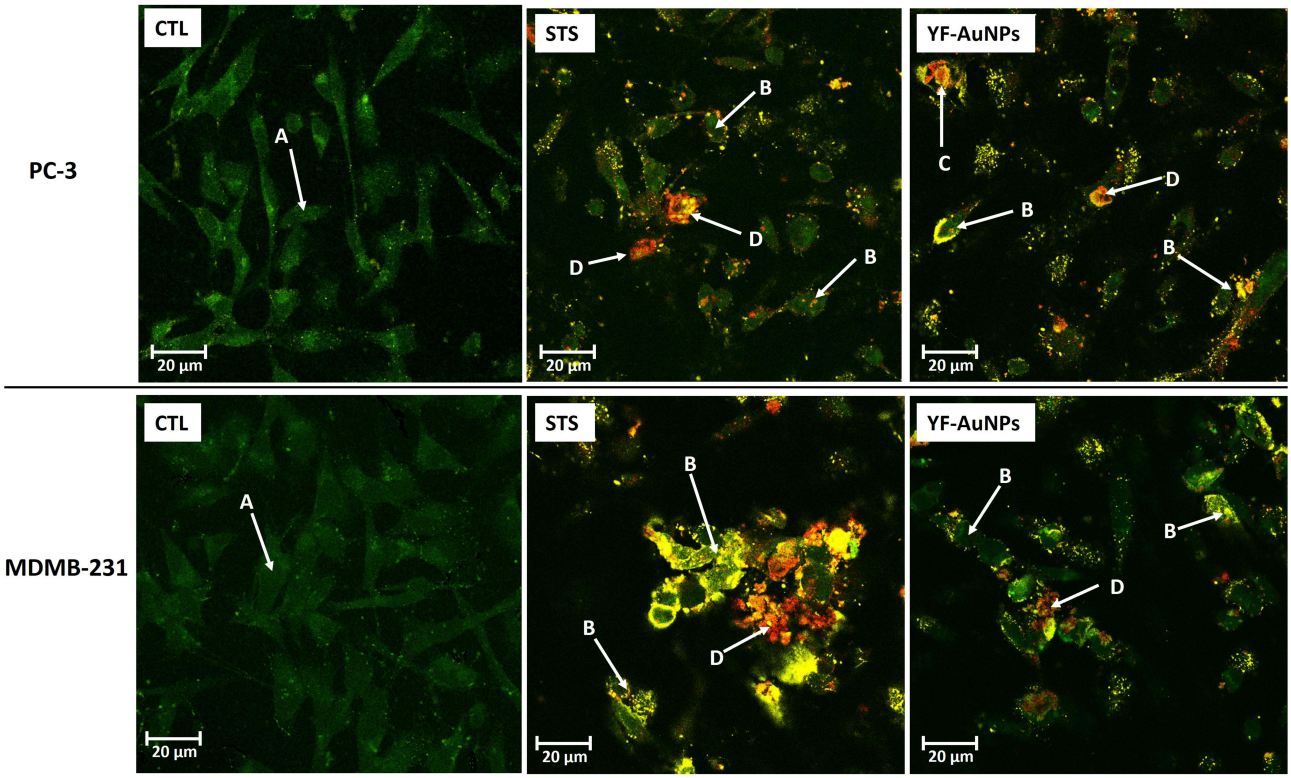

Figure 15 Confocal microscopy images of apoptosis and necrosis of PC-3 and MDAMB 231 cells with no treatment (CTL) and after treatment with staurosporine (STS) and YF-AuNPs. (**A**) Healthy cells, (**B**) early apoptosis, (**C**) late-apoptosis, and (**D**) necrotic cells.

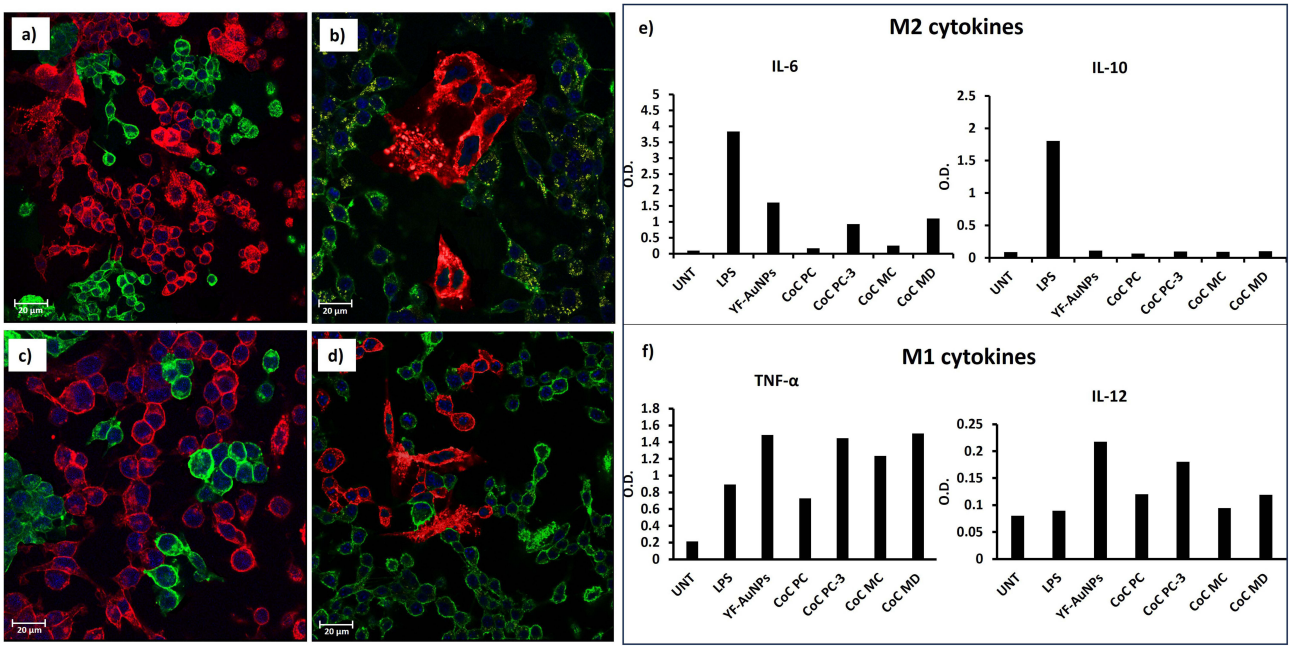

Figure 16 Confocal microscopy images of (**a**) co-culture of PC-3 cell lines (red) and naive RAW 264.7 macrophage cell line (green); (**b**) co-culture of PC-3 cell lines (red) and YF-AuNPs pre-treated RAW 264.7 macrophage cell line (green); (**c**) co-culture of MDAMB 231 cell lines (red) and naive RAW 264.7 macrophage cell line (green); and (**d**) co-culture of MDAMB 231 cell lines (red) and YF-AuNPs pre-treated RAW 264.7 macrophage cell line (green) demonstrated an ability of YF-AuNPs activated RAW 264.7 macrophage cell line to suppress the growth of prostate and breast tumor cells. Immunomodulatory activity of YF-AuNPs showed (**e**) reduced levels of pro-tumor cytokines (IL-6 and IL-10) and (**f**) elevated levels of anti-tumor cytokines (TNF-α and IL-12) indicative of a polarization shift in the macrophage phenotype from pro-tumor M2 to anti-tumor M1.

Abbreviations: UNT, untreated; LPS, Lipopolysaccharide; CoC PC, co-culture PC-3 + naïve RAW 264.7 control; CoC MC, co-culture MDAMB 231 + naive RAW 264.7 control; CoC PC-3, co-culture PC-3 + YF-AuNPs treated RAW 264.7; CoC MD, co-culture MDAMB 231 + YF-AuNPs treated RAW 264.7.

addition, there is evidence that phytochemicals derived from *Y. filamentosa* suppress NF-κB—a major cell signaling pathway directly involved in various inflammatory diseases including all cancers. Dietary saponins, derived from phytochemicals from *Y. filamentosa*, are being used to reduce blood cholesterol levels through binding to cholesterol excreted in the bile in hypercholesterolemic individuals, thus inhibiting entero-hepatic cholesterol recycling.[30] Saponins can affect cellular membrane permeability by forming complexes with cholesterol in mucosal cell membranes thereby causing damage to the integrity of the membranes. An important part of our investigation was to elucidate the phytochemical constitution of aqueous extracts of *Y. filamentosa* through detailed LC-MS/MS analysis. Our LC-MS/MS analysis has revealed that the major phytochemical chemical constituents in the aqueous extracts of *Y. filamentosa* are Timosaponin BII followed by arginine, L-pyroglutamic acid, glycosylated compounds, 3-alkylindoles, pyridine derivatives, and flavonoid-7-O-glycosides as shown in Figures 1 and 2.

Our green nanotechnology approaches have utilized the power of electron-rich phytochemical cocktail from *Y. filamentosa* as a powerful reservoir of electrons aimed at transforming gold precursors into the corresponding phytochemical-encapsulated gold nanoparticles. It is important to recognize that the green nanotechnology process imbibes Ayurvedic holistic medicine principles without utilizing any toxic human-made chemicals (except the gold precursor) in the overall formulation of *Y. filamentosa* phytochemical encapsulated new nanomedicine agent YF-AuNPs. In additional experiments, we have utilized the FDA approved plant-derived gum arabic (GA) protein to further stabilize-AuNPs to produce GAYF-AuNPs. Incorporation of gum arabic on the gold nanoparticulate surface affords optimum in vitro and in vivo stability against agglomeration under the complex biological in vivo conditions.[2,14,15,18–20,54–59] As we have utilized nanotechnology to encapsulate Ayurvedically-relevant phytochemicals from *Y. filamentosa*, we have coined the term nano-Ayurvedic medicine for this medical approach. The US Patents and Trademarks office has recently granted the first ever patent for our invention on nano-Ayurvedic medicine.[33,34] Rigorous experimental parameters were performed for the optimization of the synthesis to achieve stabilized YF-AuNPs capable of providing adjuvant therapeutic benefits through delivering potent doses of both the phytochemicals and nanoparticles.

Complete characterization of both *Y. filamentosa* gold nanoparticles (YF-AuNPs) and gum arabic stabilized *Y. filamentosa* gold nanoparticles (GAYF-AuNPs) has been carried out using a combination of spectrophotometric and electron microscopic techniques. Ultraviolet-visible (UV-Vis) spectroscopy of these nanoparticles indicated surface plasmon resonance (SPR) absorptions at 536 and 540 nm, for YF-AuNPs and GAYF-AuNPs, respectively (Figure 3). The proposed mechanism of *Y. filamentosa* extract reduces Au^{3+} ions to Au^{0}, thereby produces corresponding *Y. filamentosa* gold nanoparticles (YF-AuNPs) as shown in Figure 4. This was supported by FTIR and XRD data that revealed interaction of *Y. filamentosa* extract phytochemicals with the gold nanoparticle surface, acting as both a reducing and stabilizing ligand for the nanoparticles. The XRD analysis of gold nanoparticles demonstrated four peaks corresponding to standard Bragg reflections (111), (200), (220), and (311) of face centers cubic lattice crystalline AuNPs (Figure 5a). A moderate zeta potential of −19 mV and −20 mV for YF-AuNPs and GAYF-AuNPs; respectively, confirmed the optimum in vitro/in vivo stability of these nanoparticles for use in biomedical applications. This means that the nanoparticles are not strongly repelled from each other, and they are therefore more likely to aggregate or clump together. Additionally, the zeta potential provides crucial information about the fate and interaction (nano-bio) of nanoparticle in different biological media.

The moderate −19 and −20 mV zeta is beneficial and favors the enhanced permeability and retention (EPR) effect because nanoparticles with a low zeta potential are more likely to be taken up by cancer cells.[60,61] Once internalized in the cancer cell, the nanoparticles can release bioactive *Y. filamentosa* phytochemicals. Furthermore, the negative zeta potential affords evasion from identification by the phagocytic system resulting in low serum protein binding and potentially longer circulation. Polydispersity index (PDI) of 0.3 and 0.2, for YF-AuNPs and GAYF-AuNPs, respectively, further confirmed excellent quality of nanoparticles produced through green nanotechnology and 100% reproducible processes. To assess the stability and suitability of YF-AuNPs and GAYF-AuNPs nanoparticles for use under in vivo conditions, we have further performed detailed stability evaluations of both nanomedicine agents YF-AuNPs and GAYF-AuNPs. These investigations involved incubating aliquots of YF-AuNPs and GAYF-AuNPs, separately, with solutions of 1% NaCl, cysteine, human serum albumin (HSA), and bovine serum albumin (BSA)—and estimating stability of nanoparticles based on the retention of surface plasmon resonance (SPR) peaks in the UV-vis spectroscopy analysis.

As shown in Figure 6, our investigations, unequivocally, provide evidence on the excellent stability of both YF-AuNPs and GAYF-AuNPs in various biological media as well as at pH 5 and 7 over a period of seven days. Our investigations provide credible evidence that green nanotechnology approaches, as described above, produce biocompatible YF-AuNPs and GAYF-AuNPs nanomedicine agent with optimum stability.

Transmission electron microscopic (TEM) data as shown in Figure 7 (and in Table 1) provided conclusive proof that the cocktail of phytochemicals corona, on both YF-AuNPs and GAYF-AuNPs, affords excellent in vitro stability without any agglomerations. Hydrodynamic size measurements through dynamic light scattering (DLS) indicated sizes of 335 ± 10 nm; and 188 ± 5 nm, for YF-AuNPs and GAYF-AuNPs, respectively. The hydrodynamic size is higher than the metal core size at 14 ± 5 nm and 10 ± 5 nm obtained by TEM, signifying robust surface coating of *Y. filamentosa* phytochemicals onto the surface of nanoparticles —further confirming the robust corona formed from the cocktail of phytochemicals from *Y. filamentosa* on gold nanoparticulate surfaces. It is also important to note that previous reports by Krishnamurthy et al[62] produced gold nanoparticles using *Y. filamentosa* leaf extract, with sub-optimal polydispersity of AuNPs ranging from 20 to 300 nm size and also comprised of complex mixtures of nanoparticulate geometric morphologies. In sharp contrast, our green nanotechnology approaches have resulted in the formulation of robust *Y. filamentosa* phytochemical coronas on both YF-AuNPs and gum arabic stabilized GAYF-AuNPs with near monodisperse characteristics. Our green nanotechnology approaches, therefore, provide compelling evidence on highly effective pathways toward the development of biocompatible nano-Ayurvedic medicine agents for potential applications in oncology and in the treatment of various diseases.

Tumor cell targeting ability of YF-AuNPs was studied by incubating this nanomedicine agent with breast (MDAMB-231), and prostate (PC-3) cancer cells. These tumor cells were subsequently analyzed through confocal microscopy to probe if the *Y. filamentosa* phytochemicals functionalized gold nanoparticles (YF-AuNPs) target tumor cells in addition to macrophage cell lines. As shown in Figures 8–11, YF-AuNPs nanomedicine agent targets breast and prostate tumor cells, and macrophage cell lines with excellent propensity to internalize through endocytosis via vacuoles housing YF-AuNPs and maintains their integrity (size and shape) inside these cells. The confocal and transmission electron microscopic data, therefore, fully corroborate the excellent antitumor activities of this nanomedicine agent as depicted in Figures 8–11.

Antitumor assays of YF-AuNPs and gum arabic stabilized GAYF-AuNPs nano-Ayurvedic medicine agents showed inhibition of tumor cell growth. Timosaponin BII, a major phytochemical from *Y. filamentosa* has shown limited pharmacological bioactivity.[29,39] There are very few reports on the application of cocktail of phytochemicals from this plant toward the design of herbal or Ayurvedic medicinal drugs. We hypothesized that incorporation of timosaponin BII, and a myriad of flavonoid-7-O-glycosides and glycosylated compounds—all found in good abundance in *Y. filamentosa* —onto gold nanoparticulate surfaces, would not only enhance their bioavailability but would also provide effective avenues to target cancers at cellular levels. Our overall rationale for this hypothesis stemmed from the fact that creation of a strong and robust corona of timosaponin BII, myriad of flavonoid-7-O-glycosides and glycosylated compounds on gold nanoparticulate surfaces would allow the development of a new range of anti-tumor nanomedicine agents with optimum antitumor activities through the modulation of reactive oxygen species (ROS)-scavenging enzymes, induction of apoptosis, autophagy, and thus resulting in inhibition of cancer cell proliferation.

To validate the above hypothesis, we have performed detailed MTT cell proliferation assays of YF-AuNPs using breast (MDAMB-231), and prostate (PC-3) cancer cell lines. As shown in Figures 12 and 13, Table 2, the YF-AuNPs nanomedicine agent showed excellent antitumor activities against both the prostate and breast tumors. It is important to recognize that the antitumor activities of YF-AuNPs are comparable to that of the FDA approved cisplatin cancer therapy agent. Comparisons of toxicities of the YF-AuNPs nanomedicine agent and cisplatin against HAEC normal cells (Figure 14) revealed vitally important observation that YF-AuNPs nanomedicine agent selectively targets tumor cells sparing normal cells—an approach that would reduce systemic toxicity of cancer therapeutic agents. On the other hand, the FDA-approved cisplatin cancer therapy agent showed indiscriminate toxicity to both the tumor and normal cells. The confocal images of PC-3 and MDAMB-231 cells in Figure 15 revealed distinct stages of apoptosis. Early apoptotic cells were marked by a vivid yellow fluorescence, while late apoptotic cells displayed a yellow-orange hue. Necrotic cells were identifiable by their uniform orange or red nuclei. These observations indicated the presence of typical signs of

apoptosis in both cell lines, including cell shrinkage, the formation of apoptotic bodies, and membrane blebbing. Similar results have been reported by Khoobchandani et al[24] and Kumari et al[60] where mangiferin and curcumin nanoparticles induced apoptosis in PC-3 and MDAMB 231 cancer cells, respectively.

Targeting of M2-Like Protumor Macrophage Cell Lines by YF-AuNPs Nano-Ayurvedic Medicine Agents

It is well known that tumor-associated macrophages (TAMs), in most tumors, can transition between an anti-inflammatory promoting a pro-tumorigenic M2-like phenotype and a pro-inflammatory and anti-tumorigenic M1-phenotype manifesting effective tumor treatment state.[63–65] Overwhelming clinical evidence suggests the importance of macrophage cell lines in the prognosis of patients with a wide range of cancers at various stages of the disease.[66–70] Our hypothesis-driven approach has been to experimentally validate whether certain types of phytochemical functionalized gold nanoparticles display macrophage cell line polarization through targeting the pro-tumor M2 macrophage cell lines. In order to conduct preliminary investigations on the ability of the aforementioned gold nanoparticles on their propensity to target M2-like protumor macrophage cell lines, we have chosen RAW 264.7 macrophage cell lines.[26,27] RAW 264.7, by default, manifests M2-like protumor characteristics within the tumor microenvironment and is directly involved in the growth, propagation, and metastases of most human/mammalian tumors.[26] As shown in Figure 16, a significant difference in cellular density between cancer cells treated with naïve macrophage cell lines and those treated with YF-AuNPs pretreated macrophage cell lines. The latter showed a lower cell density, indicating a potential inhibitory effect of YF-AuNPs pretreated macrophage cell line on cancer cell growth. This finding is promising because it suggests that YF-AuNPs may have the ability to modulate the cytokine profile of RAW 264.7 macrophage cell line exhibiting immunomodulatory properties.

Additionally, the impact of YF-AuNPs on the secretion of macrophage-polarizing cytokines revealed that RAW 264.7 macrophages treated with YF-AuNPs exhibited increased levels of anti-tumor cytokines, including TNF-α and IL-12, while showing reduced levels of pro-tumor cytokines, such as IL-6 and IL-10. These results are highly significant as they suggest that YF-AuNPs can modulate the immune response by promoting the production of anti-tumor cytokines and suppressing pro-tumor cytokines. In contrast, the reduction in pro-tumor cytokines, IL-6 and IL-10, indicates a shift in the macrophage phenotype from pro-tumor M2 to anti-tumor M1.

The results underscore the ability of YF-AuNPs to effectively target pro-tumor macrophage cell lines and modulate the immune response. By influencing macrophage polarization and cytokine secretion, YF-AuNPs show promise as a potential therapeutic approach in treating various types of cancers. Further research and in vivo studies are essential to explore the full potential of YF-AuNPs in cancer immunotherapy. Because, tumor progression and consequent immune response events are intricately linked, our investigations, as outlined in various sections of this paper, have revealed that *Y. filamentosa* phytochemicals encapsulated gold nanoparticles are effective immunomodulatory agents as they exhibited efficient targeting of macrophage cell lines within the tumor microenvironment. The outstanding anti-tumor efficacy of *Y. filamentosa* phytochemicals encapsulated gold nanoparticles can therefore be explained through immunomodulatory intervention of this new generation of nano-Ayurvedic medicine agents. It is important to recognize that *Y. filamentosa* phytochemicals encapsulated gold nanoparticles exhibited substantially lower toxicity toward normal cells as compared to the FDA approved cisplatin. These favorable cancer immunotherapeutic and lower toxicity profiles of *Y. filamentosa* phytochemicals encapsulated gold nanoparticles present unprecedented potential for their applications in oncology.

Conclusions

Our green nanotechnology approaches, as described in this article, qualify to be referred to as a "Zero Carbon Emission" green and sustainable drug design process because no toxic human-made chemicals were utilized in the overall nanomedicine production scheme. The simultaneous production of gold nanoparticles and encapsulation of a plethora of phytochemicals from *Y. filamentosa*, including, timosaponin BII, glycosylated compounds, and flavonoid-7-O-glycosides, on the surface of gold nanoparticles provides an efficient way to produce biocompatible nanomedicine agents. Overall, our approach presents realistic possibilities to fulfill the tremendous potential of plant-based

phytochemicals in the creation of herbal and nano-Ayurvedic immunomodulatory nanomedicine-based therapeutic agents for treating cancer and other diseases.

Abbreviations

YF, *Yucca filamentosa*; YF-AuNPs, *Y. filamentosa* phytochemicals encapsulated gold nanoparticles; GA, gum arabic; GAYF-AuNPs, gum arabic stabilized *Y. filamentosa* phytochemicals encapsulated gold nanoparticles; $NaAuCl_4 \cdot 2H_2O$, sodium tetrachloroaurate(III) dihydrate 99%; Cys, DL-cysteine 97%; BSA, bovine serum albumin; HSA, human serum albumin; FBS, fetal bovine serum; NaCl, sodium chloride; PBS, phosphate buffered saline; HBSS, Hanks' balanced salt solution; DAPI, 4',6-diamidino-2-phenylindole; His, L-histidine 98%; MTT, 3-(4,5-dimethylthiazol-2-yl)-2,5-diphenyl-tetrazolium bromide; WGA, wheat germ agglutinin, Oregon Green® 488 conjugate; DMEM, Dulbecco's modified eagle's medium; RPMI, Roswell Park Memorial Institute; PC-3, prostate cancer cells; MDAMB-231, breast cancer cells; DMSO, dimethyl sulfoxide; DLS, dynamic light scattering; LC-MS/MS, liquid chromatography with tandem mass spectrometry; UV-vis, ultraviolet–visible spectroscopy; PDI, polydispersity index; TEM, transmission electron microscopy; IC_{50}, half-maximal inhibitory concentration.

Ethics Statement

Yucca filamentosa, collected from the University of Missouri, Columbia campus, USA, was identified and authenticated by Dr K. H. Clary. A voucher specimen (BC:MO-2267845/A:3345883) was obtained from the Missouri Botanical Garden Herbarium.

Acknowledgments

This work has been supported by funding obtained through the Institute of Green Nanotechnology and the Department of Radiology, University of Missouri Medical School, University of Missouri, Columbia, Missouri, USA. The authors would like to thank Ms Nya Hall for assistance in performing the apoptosis/necrosis, immunomodulatory, co-culture investigations.

Disclosure

The authors report no conflicts of interest in this work.

References

1. WHO. WHO establishes the global centre for traditional medicine in India; 2022. Available from: https://www.who.int/news/item/25-03-2022-who-establishes-the-global-centre-for-traditional-medicine-in-india. Accessed September 28, 2022.
2. Kattumuri V, Katti KK, Bhaskaran S, et al. Gum arabic as a phytochemical construct for the stabilization of gold nanoparticles: in vivo pharmacokinetics and X-ray-contrast-imaging studies. *Small*. 2007;3(2):333–341. doi:10.1002/smll.200600427
3. Mohan RR, Sinha S, Katti KV, Kannan R, Stapleton WM, Schultz GS. Evaluation of polymeric- and gold-nanoparticles for gene delivery in the cornea. *Invest Ophthalmol Vis Sci*. 2007;48(13):2733.
4. Fent GM, Casteel SW, Kim DY, et al. Biodistribution of maltose and gum arabic hybrid gold nanoparticles after intravenous injection in juvenile swine. *Nanomedicine*. 2009;5(2):128–135. doi:10.1016/j.nano.2009.01.007
5. Chanda N, Shukla R, Katti KV, Kannan R. Gastrin releasing protein receptor specific gold nanorods: breast and prostate tumor avid nanovectors for molecular imaging. *Nano Lett*. 2009;9(5):1798–1805. doi:10.1021/nl8037147
6. Katti KK, Kattumuri V, Bhaskaran S, Katti KV, Kannan R. Facile and general method for synthesis of sugar-coated gold nanoparticles. *Int J Green Nanotechnol Biomed*. 2009;1(1):B53–B59. doi:10.1080/19430850902983848
7. Nune SK, Chanda N, Shukla R, et al. Green nanotechnology from tea: phytochemicals in tea as building blocks for production of biocompatible gold nanoparticles. *J Mater Chem*. 2009;19(19):2912–2920. doi:10.1039/b822015h
8. Katti KK, Chanda N, Shukla R, et al. Green nanotechnology from cumin phytochemicals: generation of biocompatible gold nanoparticles. *Int J Green Nanotechnol Biomed*. 2009;1(1):B39–B52.
9. Chanda N, Kattumuri V, Shukla R, et al. Bombesin functionalized gold nanoparticles show in vitro and in vivo cancer receptor specificity. *Proc Natl Acad Sci*. 2010;107(19):8760–8765. doi:10.1073/pnas.1002143107
10. Shukla R, Chanda N, Zambre A, Upendran A, Katti K, Kulkarni RR. Laminin receptor specific therapeutic gold efficacy in treating prostate cancer. *Proc Natl Acad Sci*. 2012;109(31):12426–12431. doi:10.1073/pnas.1121174109
11. Khoobchandani M, Zambre A, Katti KK, ho LC, Katti KVK. Green nanotechnology from Brassicaceae: development of broccoli phytochemicals – encapsulated gold nanoparticles and their applications in nanomedicine. *Int J Green Nanotechnol*. 2013;1:1–15. doi:10.1177/1943089213509474
12. Gamal-Eldeen AM, Moustafa D, El-Daly SM, et al. Photothermal therapy mediated by gum Arabic-conjugated gold nanoparticles suppresses liver preneoplastic lesions in mice. *J Photochem Photobiol B*. 2016;163:47–56. doi:10.1016/j.jphotobiol.2016.08.009

13. Geraldes AN, Alves A, Leal J, et al. Green nanotechnology from plant extracts: synthesis and characterization of gold nanoparticles. *ANP*. 2016;5(3):176–185. doi:10.4236/anp.2016.53019
14. Gamal-Eldeen AM, Moustafa D, El-Daly SM, et al. Gum Arabic-encapsulated gold nanoparticles for a non-invasive photothermal ablation of lung tumor in mice. *Biomed Pharmacother*. 2017;89:1045–1054. doi:10.1016/j.biopha.2017.03.006
15. Katti KV, Khoobchandani M, Thipe VC, et al. Prostate tumor therapy advances in nuclear medicine: green nanotechnology toward the design of tumor specific radioactive gold nanoparticles. *J Radioanal Nucl Chem*. 2018;318(3):1737–1747. doi:10.1007/s10967-018-6320-4
16. Tangthong T, Piroonpan T, Thipe VC, et al. Water-soluble chitosan conjugated DOTA-bombesin peptide capped gold nanoparticles as a targeted therapeutic agent for prostate cancer. *Nanotechnol Sci Appl*. 2021;14(14):69–89. doi:10.2147/NSA.S301942
17. Thipe VC, Karikachery AR, Çakılkaya P, et al. Green nanotechnology—an innovative pathway towards biocompatible and medically relevant gold nanoparticles. *J Drug Deliv Sci Technol*. 2022;70:103256.
18. Maziero J, Thipe V, Rogero S, et al. Species specific in vitro and in vivo evaluation of toxicity of silver nanoparticles stabilized with arabic gum protein. *Int J Nanomedicine*. 2020;15:7359–7376. doi:10.2147/IJN.S250467
19. De Canha MN, Thipe VC, Katti KV, et al. The activity of gold nanoparticles synthesized using helichrysum odoratissimum against cutibacterium acnes biofilms. *Front Cell Dev Biol*. 2021;9(1):1–16. doi:10.3389/fcell.2021.675064
20. Thipe VC, Amiri KP, Bloebaum P, et al. Development of resveratrol-conjugated gold nanoparticles: interrelationship of increased resveratrol corona on anti-tumor efficacy against breast, pancreatic and prostate cancers. *Int J Nanomedicine*. 2019;14:4413–4428. doi:10.2147/IJN.S204443
21. Thipe VC, Njobeh PB, Mhlanga SD. Optimization of commercial antibiotic agents using gold nanoparticles against toxigenic Aspergillus spp. *Mater Today Proc*. 2015;2(7):4136–4148. doi:10.1016/j.matpr.2015.08.044
22. Khoobchandani M, Katti KK, Karikachery AR, et al. New approaches in breast cancer therapy through green nanotechnology and nano-ayurvedic medicine - pre-clinical and pilot human clinical investigations. *Int J Nanomedicine*. 2020;15:181–197. doi:10.2147/IJN.S219042
23. Lambrechts IA, Thipe VC, Katti KV, et al. Targeting acne bacteria and wound healing in vitro using Plectranthus aliciae, rosmarinic acid, and tetracycline gold nanoparticles. *Pharmaceuticals*. 2022;15(8):933. doi:10.3390/ph15080933
24. Khoobchandani M, Khan A, Katti KK, et al. Green nanotechnology of MGF-AuNPs for immunomodulatory intervention in prostate cancer therapy. *Sci Rep*. 2021;11(1):16797. doi:10.1038/s41598-021-96224-8
25. Sibuyi NRS, Thipe VC, Panjtan-Amiri K, Meyer M, Katti KV. Green synthesis of gold nanoparticles using acai berry and elderberry extracts and investigation of their effect on prostate and pancreatic cancer cells. *BJGP Open*. 2021;8:1–8.
26. Plock A, Beyer G, Hiller K, et al. Application of MS and NMR to the structure elucidation of complex sugar moieties of natural products: exemplified by the steroidal saponin from *Yucca filamentosa* L. *Phytochemistry*. 2001;57(3):489–496. doi:10.1016/s0031-9422(01)00035-8
27. Culhuac EB, Maggiolino A, Elghandour MMMY, De Palo P, Salem AZM. Antioxidant and anti-inflammatory properties of phytochemicals found in the yucca genus. *Antioxidants*. 2023;12(3):574. doi:10.3390/antiox12030574
28. Adegbeye MJ, Elghandour MMMY, Monroy JC, et al. Potential influence of yucca extract as feed additive on greenhouse gases emission for a cleaner livestock and aquaculture farming - A review. *J Clean Prod*. 2019;239(3):118074. doi:10.1016/j.jclepro.2019.118074
29. Jiménez GG, Durán AG, Macías FA, Simonet AM. Structure, bioactivity and analytical methods for the determination of yucca saponins. *Molecules*. 2021;26(17):5251. doi:10.3390/molecules26175251
30. Cheeke PR, Piacente S, Oleszek W. Anti-inflammatory and anti-arthritic effects of yucca schidigera: a review. *J Inflamm*. 2006;3. doi:10.1186/1476-9255-3-6
31. Hans CP, Sharma N, Downey E, Khoobchandani M, Katti K, Katti KV. Mangiferin conjugated gold nanoparticles protect against the development of abdominal aortic aneurysm in an apoe−/− mouse model. *JVS Vasc Sci*. 2022;3:16–17.
32. Al-Yasiri AY, Khoobchandani M, Cutler CS, et al. Mangiferin functionalized radioactive gold nanoparticles (MGF-198AuNPs) in prostate tumor therapy: green nanotechnology for production, in vivo tumor retention and evaluation of therapeutic efficacy. *Dalton Trans*. 2017;46(42):14561–14571. doi:10.1039/C7DT00383H
33. Katti K, Cutler C, Khoobchandani M, Katti K. The curators of the university of Missouri. Mangiferin encapsulated gold nanoparticles, fabrication methods and cancer therapeutic methods. United States patent US 11426357B2. 2022 Aug 30.
34. Katti K, Menka K, Kavita K, Chintamani J, Alsam K, Mutalik V. The curators of the University of Missouri. Ayurvedic encapsulated gold nanoparticles, fabrication methods and cancer therapeutic methods. United States patent US 011547720B2; 2023 Jan 10.
35. Patil-Bhole T, Wele A, Gudi R, et al. Nanostructured gold in ancient ayurvedic calcined drug 'swarnabhasma. *J Ayurveda Integr Med*. 2021. doi:10.1016/j.jaim.2021.06.017
36. Pal D, Sahu CK, Haldar A. Bhasma: the ancient Indian nanomedicine. *J Adv Pharm Technol Res*. 2014;5(1):4–12. doi:10.4103/2231-4040.126980
37. Shingadiya R, Chaudhary S, Joshi K, Bedarkar P, Patgiri B, Prajapati P. Evidence-based safety and efficacy of ayurvedic herbo-metallic preparations containing gold, iron, and mercury with special reference to pediatrics. *Med J DY Patil Univ*. 2017;10(3):222–228. doi:10.4103/0975-2870.206579
38. Lei Z, Jing L, Qiu F, et al. Construction of an ultrahigh pressure liquid chromatography-tandem mass spectral library of plant natural products and comparative spectral analyses. *Anal Chem*. 2015;87(14):7373–7381. doi:10.1021/acs.analchem.5b01559
39. Lin N, Liu B, Zhang J, et al. Acute toxicity, 28-day repeated-dose toxicity and toxicokinetic study of timosaponin BII in rats. *Regul Toxicol Pharmacol*. 2017;90(27):244–257. doi:10.1016/j.yrtph.2017.09.021
40. Wang N, Xu P, Wu R, et al. Timosaponin BII improved osteoporosis caused by hyperglycemia through promoting autophagy of osteoblasts via suppressing the mTOR/NFκB signaling pathway. *Free Radic Biol Med*. 2021;171(April):112–123. doi:10.1016/j.freeradbiomed.2021.05.014
41. Zhou F, Liu BF, Wang C, et al. Acute toxicity, 28-day repeated-dose toxicity and toxicokinetic study of timosaponin BII in beagle dogs. *J Asian Nat Prod Res*. 2022;24(9):860–876.
42. Ceylan R, Demirbas A, Ocsoy I, Aktumsek A. Green synthesis of silver nanoparticles using aqueous extracts of three Sideritis species from Turkey and evaluations bioactivity potentials. *Sustain Chem Pharm*. 2021;21(November 2020):100426. doi:10.1016/j.scp.2021.100426
43. Albeladi SSR, Malik MA, Al-Thabaiti SA. Facile biofabrication of silver nanoparticles using Salvia officinalis leaf extract and its catalytic activity towards Congo red dye degradation. *J Mater Res Technol*. 2020;9(5):10031–10044. doi:10.1016/j.jmrt.2020.06.074
44. Unal IS, Demirbas A, Onal I, Ildiz N, Ocsoy I. One step preparation of stable gold nanoparticle using red cabbage extracts under UV light and its catalytic activity. *J Photochem Photobiol B*. 2020;204(August 2019):111800. doi:10.1016/j.jphotobiol.2020.111800

45. Roma-Rodrigues C, Mendes R, Baptista PV, Fernandes AR. Targeting tumor microenvironment for cancer therapy. *Int J Mol Sci*. 2019;20(4):840. doi:10.3390/ijms20040840
46. Daßler-Plenker J, Küttner V, Egeblad M. Communication in tiny packages: exosomes as means of tumor-stroma communication. *Biochim Biophys Acta Rev Cancer*. 2020;1873(2):188340. doi:10.1016/j.bbcan.2020.188340
47. Tiwari A, Trivedi R, Lin SY. Tumor microenvironment: barrier or opportunity towards effective cancer therapy. *J Biomed Sci*. 2022;29(1):83. doi:10.1186/s12929-022-00866-3
48. Baghban R, Roshangar L, Jahanban-Esfahlan R, et al. Tumor microenvironment complexity and therapeutic implications at a glance. *Cell Commun Signaling*. 2020;18(1):59. doi:10.1186/s12964-020-0530-4
49. Jin MZ, Jin WL. The updated landscape of tumor microenvironment and drug repurposing. *Signal Transduct Target Ther*. 2020;5(1):166. doi:10.1038/s41392-020-00280-x
50. Chen PC, Cheng HC, Wang J, et al. Prostate cancer-derived CCN3 induces M2 macrophage infiltration and contributes to angiogenesis in prostate cancer microenvironment. *Oncotarget*. 2014;5(6):1595–1608. doi:10.18632/oncotarget.1570
51. Zhang M, Pan X, Fujiwara K, et al. Pancreatic cancer cells render tumor-associated macrophages metabolically reprogrammed by a GARP and DNA methylation-mediated mechanism. *Signal Transduct Target Ther*. 2021;6(1):1.
52. Jadrzejewski T, Pawlikowska M, Sobociåska J, Wrotek S. Protein-bound polysaccharides from coriolus versicolor fungus disrupt the crosstalk between breast cancer cells and macrophages through inhibition of angiogenic cytokines production and shifting tumour-associated macrophages from the M2 to M1 subtype. *Cell Physiol Biochem*. 2020;54(4):615–628.
53. Deng D, Patel R, Chiang CY, Hou P. Role of the tumor microenvironment in regulating pancreatic cancer therapy resistance. *Cells*. 2022;11(19):2952. doi:10.3390/cells11192952
54. Sinha S, McKnight D, Katti KV, et al. Gold nanoparticles stabilized in gum arabic for corneal gene therapy. *Invest Ophthalmol Vis Sci*. 2008;49(13):4787.
55. Gamal-Eldeen AM, Moustafa D, El-Daly SM, Katti KV. P0131 efficacy of gum arabic-conjugated gold nanoparticles as a photothermal therapy for lung cancer: in vitro and in vivo approaches. *Eur J Cancer*. 2014;50:e46. doi:10.1016/j.ejca.2014.03.175
56. Bryan JN, Henry CJ, Boote E, et al. Gum arabic-coated radioactive gold nanoparticles cause no short-term local or systemic toxicity in the clinically relevant canine model of prostate cancer. *Int J Nanomedicine*. 2014;9(October):5001–5011. doi:10.2147/IJN.S67333
57. Chanda N, Upendran A, Boote EJ, et al. Gold nanoparticle based X-ray contrast agent for tumor imaging in mice and dog: a potential nano-platform for computer tomography theranostics. *J Biomed Nanotechnol*. 2014;10(3):383–392. doi:10.1166/jbn.2014.1725
58. Cutler C, Al-Yasiri A, Kuchuk M, et al. Comparison of in vivo uptake of radioactive gold nanoparticles formulated using phytochemicals. *J Nucl Med*. 2015;56(supplement 3):1267 LP–1267.
59. Kannan R, Zambre A, Chanda N, et al. Functionalized radioactive gold nanoparticles in tumor therapy. *Wiley Interdiscip Rev Nanomed Nanobiotechnol*. 2012;4(1):42–51. doi:10.1002/wnan.161
60. Kumari M, Sharma N, Manchanda R, et al. PGMD/curcumin nanoparticles for the treatment of breast cancer. *Sci Rep*. 2021;11(1):1–17. doi:10.1038/s41598-021-81701-x
61. Fan D, Cao Y, Cao M, Wang Y, Cao Y, Gong T. Nanomedicine in cancer therapy. *Signal Transduct Target Ther*. 2023;8(1). doi:10.1038/s41392-023-01536-y
62. Krishnamurthy S, Esterle A, Sharma NC, Sahi SV. Yucca-derived synthesis of gold nanomaterial and their catalytic potential. *Nanoscale Res Lett*. 2014;9(1):1–9. doi:10.1186/1556-276X-9-627
63. Mantovani A, Allavena P, Marchesi F, Garlanda C. Macrophages as tools and targets in cancer therapy. *Nat Rev Drug Discov*. 2022;21(11):799–820. doi:10.1038/s41573-022-00520-5
64. Balakrishnan A, Vig M, Dubey S. Role of myeloid cells in the tumor microenvironment. *J Cancer Metastasis Treat*. 2022;8(5):27. doi:10.20517/2394-4722.2022.33
65. Boutilier AJ, Elsawa SF. Macrophage polarization states in the tumor microenvironment. *Int J Mol Sci*. 2021;22(13):6995. doi:10.3390/ijms22136995
66. Mishra AK, Banday S, Bharadwaj R, et al. Macrophages as a potential immunotherapeutic target in solid cancers. *Vaccines*. 2023;11(1):1–30.
67. Cendrowicz E, Sas Z, Bremer E, Rygiel TP. The role of macrophages in cancer development and therapy. *Cancers*. 2021;13(8):1946. doi:10.3390/cancers13081946
68. Yuan Y, Long L, Liu J, et al. The double-edged sword effect of macrophage targeting delivery system in different macrophage subsets related diseases. *J Nanobiotechnology*. 2020;18(1):1–14. doi:10.1186/s12951-020-00721-3
69. Zou Z, Lin H, Li M, Lin B. Tumor−associated macrophage polarization in the inflammatory tumor microenvironment. *Front Oncol*. 2023;13:1103149.
70. Yuan P, Xu X, Hu D, et al. Highly sensitive imaging of tumor metastasis based on the targeting and polarization of M2-like macrophages. *J Am Chem Soc*. 2023;145(14):7941–7951. doi:10.1021/jacs.2c13218